ENGINEERING TRANSACTIONS • *Engng. Trans.* • **66**, 1, 21–60, 2018
Polish Academy of Sciences • Institute of Fundamental Technological Research (IPPT PAN)
National Engineering School of Metz (ENIM) • Poznan University of Technology

Research Paper

Application of Translational Edge Restraint for Vibration Analysis of Free Edge Kirchhoff's Plate Including Rigid-Body Modes

Yogesh VERMA, Nabanita DATTA

Indian Institute of Technology
Kharagpur, India
e-mail: yogesh.nitkl@gmail.com

A comprehensive theoretical study of closed-form rigid-body modes of a free-free and translationally edge-restrained Euler-Bernoulli beam is presented. Accurate vibrational analysis of a free-free-free-free plate is not possible without the inclusion of degenerate rigid-body beam-wise admissible functions. The trivial solution(s) of the beam frequency equation produce(s) a non-trivial modeshape, which (i) satisfies the boundary conditions, (ii) has zero curvature, and (iii) is orthogonal to the other modeshapes. These frequency parameters are "trivial", i.e. they lead to zero natural frequency, since their modeshapes have no curvature. Mathematically-generated orthogonal free-free (classical) beam-wise rigid-body modeshapes, and those generated from non-classical edged beams, have been both separately used as admissible functions in the Rayleigh-Ritz method (RRM) to generate the plate natural frequencies of a free-free-free-free rectangular uniform isotropic Kirchhoff's plate. With respect to the increasing elastic support, the trifurcation and bifurcation of plate frequencies from the trivial to the flexural frequencies, is investigated. The completely free plate modeshapes are also presented. Also, combination of present closed-form rigid-body modes with polynomial functions, trigonometric functions is also demonstrated.

Key words: free edge plate; translational restraint; frequency parameter; rigid body modes; waveform coefficients.

Notations

- a – length of the plate [m],
- A – cross-sectional area [m^2],
- b – breadth of the plate [m],
- β – wave number of beam vibration [1/m],
- βL – frequency parameter of beam [–],
- $\beta_T L$ – frequency parameter of beam: translational [–],
- $\beta_R L$ – frequency parameter of beam: rotational [–],
- C_{ij} – Rayleigh's coefficient in plate vibration [–],

D – plate rigidity [N · m],
E – Young modulus [N/m^2],
η – non-dimensional breadth of the plate [–],
G_1, G_2, G_3, G_4 – eigen vectors of beam vibration [–],
h – thickness of the beam/plate [m],
I – area moment of inertia of cross section [m^4],
k_t – translational restraint at the edges [N/m],
k_{t0x}, k_{t1x}, k_{t0y}, k_{t1y} – translational spring constant at the four edges of the plate [N/m],
K – stiffness matrix,
K_{TR}, K_{TL} – right and left non-D translational restraint on the beam [–],
K_T – non-dimensional translational restraint on the plate edge [–],
L – length of the beam [m],
λ – aspect ratio of the plate,
m – mass per unit length of the beam [kg/m],
m_p – mass per unit area of the plate [kg/m^2],
M – mass matrix,
ν – Poisson's ratio [–],
ω – non-dimensional plate natural frequencies [–],
Ω – dimensional plate natural frequencies [rad/s],
$\phi_T(x)$ – translational rigid-body beam modeshape [–],
$\phi_R(x)$ – rotational rigid-body beam modeshape [–],
R_1, R_2, R_3, R_4 – eigen vectors of beam vibration: rotational mode [–],
ρ – density of the material [kg/m^3],
t – independent time variable [s],
T – kinetic energy of the plate [J],
T_1, T_2, T_3, T_4 – eigen vectors of beam vibration: translational mode [–],
U – potential energy of the plate [J],
$W(x, y)$ – lateral out of plane displacement of the plate [m],
W_{xi}, W_{yj} – beam modeshape in x and y-direction [m],
x – independent space variable along length of beam/plate [m],
y – independent space variable along width of plate [m],
$z(x, t)$ – beam vibration displacement [m],
$Z(x, y, t)$ – plate vibration displacement [m],
ξ – non-dimensional length, breadth of the beam/plate [–].

1. Introduction

Vibration analysis of structures with free edges poses a challenging problem. It satisfies the natural boundary conditions of zero shear force and zero bending moment, since it is not constrained against translation and rotation, respectively. In beam vibration, a hinged-free (SF) beam would have one rigid body modeshape, without any flexure, which satisfies the governing differential equation of vibration (spatial component). A free-free (FF) beam would have two rigid body modeshapes, which satisfy the governing differential equation of vibration (spatial component). Since there is no flexure, there is zero strain potential energy stored in the beam to attain such shapes, and they correspond to zero natural frequencies. However, their modeshapes participate in the beam vibration and blend with the flexural modes to reduce the net strain potential energy of the system. An example of a fully free (FFFF) plate would be a Very Large Floating Structure (VLFS), often used as floating airports. An example of an elastically supported plate would be a pneumatically stabilized platform, with the flat plate supported by pneumatic air columns and moored to the sea bed. A floating airport, with a long runway and comparatively shorted breadth, can be modelled as a free-free beam. An example of a hinged-free (SFFF) plate would be a door (of house, ship, aircraft). This work studies the vibration of such plates including the closed-form modeshapes of rigid-body "trivial" frequencies.

Leissa [12] conceded that the Free-Free-Free-Free (FFFF) plate is the most poorly behaved when studied through analytical solutions. Free edges and free corners cause difficulty in selecting accurate admissible functions into the Rayleigh-Ritz method. This fact was reiterated by Warburton and Edney [25]. Estimation of FFFF plate natural frequencies leads to large errors (∼2–13%) between numerical frequencies and those obtained by Rayleigh-Ritz method. This problem is also faced to a smaller extent by plates with one of more edges free, e.g., SSFF and SFFF plates. A free edge has bending moment and shear force zero. The lack of geometric boundary conditions weakens the accuracy of the beam-wise modeshapes, which should act as orthogonal admissible functions into the Rayleigh-Ritz method for the plate vibration analysis. When the beam boundary conditions are either FF or SF, there will be the presence of rigid-body modes in the plate analysis (Fig. 1a). A dimensionally zero frequency has a non-zero non-dimensional frequency parameter, a zero wave-number (i.e. infinite wavelength) and yet, a non-trivial modeshape. The frequency parameters of these non-flexural modes need to be accurately known for the final accuracy of the plate frequencies.

1.1. Literature review

Bassily and Dickinson [2] used degenerate beam functions (separate formulations for odd and even modes) to match the boundary conditions of the classical free edges, such that their second derivate (corresponding to the bending moment) and third derivatives (corresponding to the shear force) vanish at the ends. However, this was insufficient for rigid-body modes, which required the bending moment to be zero over the length of the beam (no curvatures, no strain potential energy). Rao and Mirza [19] studied elastically restrained

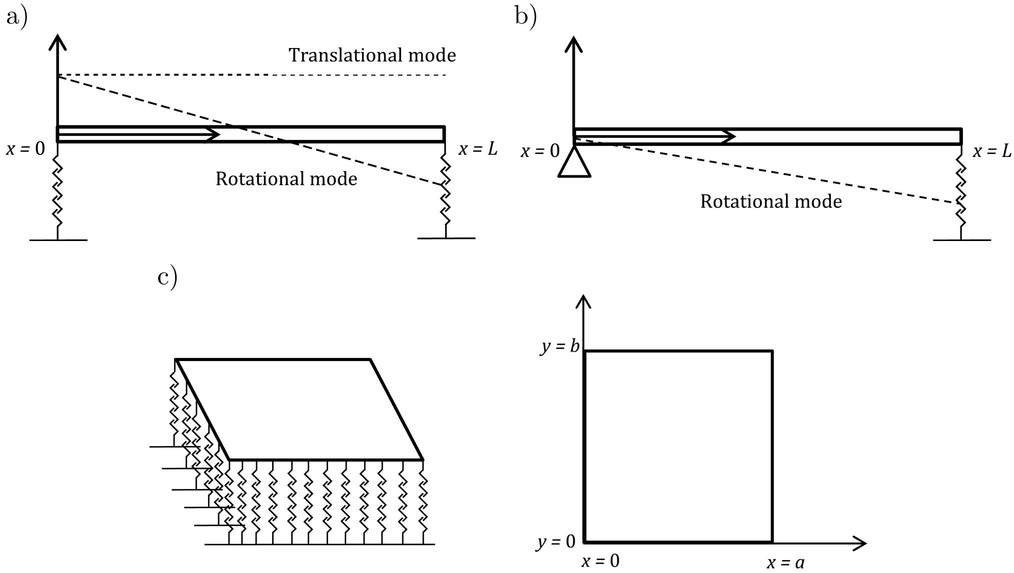

Fig. 1. a) TT beam, b) ST beam, c) elastically edge supported Kirchhoff's plate.

beams, over a very wide range of both rotational and translational edge restraints. The frequency parameters of beams with very small rotational and translational restraints were seen to approach the near-zero magnitudes, but their modeshapes where not formulated. Tang [24] numerically evaluated the modeshapes of FF beams among others with a freeware, but again, its rigid-body modes were ignored.

De Rosa and Lippiello [6] studied the free vibration of tapered beam with rotational and translational constraint by cell discretization method (CDM). Rao and Rao [20] studied the free vibration analysis of a circular plate supported on a rigid internal concentric ring with translational constraint boundary using Bessel functions. Warburton and Edney [25] studied plate vibration with (non-classical) elastically restrained edges. As the translational spring constant was reduced, the frequencies asymptoted to zero, showing rigid-body behaviour. However, the modelling of the beam admissible functions with translational edges was not explained. Dickinson and Blasio [7] used polynomials to model the degenerate beam function established by Bhat [3]. The Boundary equation method (BEM) for plate subjected to any type of boundary conditions are studied by Katsikadelis and Armenakas [11]. Bardell [1] used hierarchical finite element method and stated that the first three eigen values of a FFFF plate were zero, corresponding to the rigid-body modes of the plate. Zhou [27] studied plates with both rotational and translational restraints, but used Fourier-analysis-generated static beam functions into the Rayleigh-Ritz method. It was accepted that the admissible functions used could not degenerate to FFFF plates. Xiang *et al.* [26] studied Mindlin's plates with both edge restraints as previous work, generating their natural frequencies over a wide range of edge spring constants, without actually approaching the FFFF condition. Hurlebaus [10] derived the exact series solution for orthotropic FFFF plates, matching the exact plate boundary conditions. However, the translational rigid-body mode of the plate was deduced to have no contribution in the final vibration of the plate, countering Dickinson and Blasio [7]. Saha *et al.* [22] again used polynomial-based beam modeshapes to handle free edges, but did not converge to Leissa for higher-order frequencies. Dozio [8] used the trigonometric Ritz method to study Kirchhoff's plates with classical end conditions, using only sinusoidal admissible functions. Monterrubio and Ilanko [17] used the rigid-body admissible functions of a FF beam, but converged for only a few of the lowest frequencies of the FFFF plate, and the others had slight deviations from those of Leissa [12].

1.2. Overview of this work

As per the knowledge of the authors, limited literature is available on the rigid-body beam modeshapes of classical free-free beam which have hitherto been generated by polynomials or splines or Green's functions. Closed-form mathematical modeshapes find very limited application in solving the notorious free vibration problem of plates with one or more free edges.

This work attempts to solve the vibration of FFFF plate (and other plates with a combination of simply-supported and free edges) *indirectly* by non-classical edge conditions, i.e. the free edge is modelled as a distributed translational spring (Fig. 1c). Simultaneously, closed-form classical FF beam modes have been mathematically generated and used in the plate vibration. The *objective* of this work is as follows:

- To study the free vibration of plates with translationally constrained edges, and determine the range of translational spring constant for which the rigid-body modes participate. To generate the closed-form orthogonal rigid-body modeshapes of a free-free (FF) and hinged-free (SF) beam, satisfying the boundary conditions and having zero curvature.
- To highlight the prominence of rigid-body modes in the vibration of plates with all four edges free.

In this work, first the Euler-Bernoulli beam with translationally restrained edge(s) has been analysed for its non-classical frequency equation and modeshape (waveform) coefficients. Then, a closed-form expression for the rigid-body modeshapes have been mathematically proposed, which is used in plate vibration analysis through the Rayleigh-Ritz method. Various permutations and combinations of the edge restraint on the four sides of the plate have been studied for a large range of spring constants, asymptoting to classical plates (Leissa [12]). The prominence of the rigid-body modes have been established for FFFF and SFFF plates. The computational efficiency and accuracy of the Rayleigh-Ritz method using closed-form inputs has been noted. This leads to all possible six boundary conditions (FFFF, SFFF, SFSF, SSFF, SSSF, SSSS) which have natural boundary conditions, instead of geometric boundary conditions of a clamped (C) edge. Since a free edge is free to rotate, the rotational constraint at the edge can be assumed to be exactly zero, easing the formulation of the closed-form beam modeshapes. Researchers have often used both translational and rotational edge restraints and applied the extreme values on them to approach the classical plate conditions, e.g. Warburton and Edney [25], Rao and Mirza [19], Zhou [27], Xiang *et al.* [26]. The *novelty* here is as follows:

- ***Rigid-body beam frequency parameters***: The "trivial" solutions of beam vibration frequency equation have been accurately formulated through closed-form solutions. They yield zero natural frequencies, but participate in the plate vibration. They store no potential energy but participate in the kinetic energy of the plate, manifesting the lower (rigid-body or rigid-flexure) frequencies of the plate from the Ritz method. They also lead to the waveform coefficients, which generate the final rigid-body modeshape.
- ***"Switch" behaviour of the first non-trivial mode***: The translational rigid-body mode for a beam with both edges translationally constrained remains a trivial solution for the whole range of the spring constant. But the rotational rigid-body mode remains so for a lower range of spring constant, but then 'switches' to the flexural mode at a higher spring constant. The distinct values of the frequency parameters and the corresponding spring constant at which this 'happens is clearly demarcated by studying the four waveform coefficients.
- ***Rigid-body beam modeshapes***: the closed-form translational and rotational rigid body modeshapes of a free-free beam, and an elastically restrained end supported beam, have been separately established. The decreasing prominence of these modeshapes in the total vibration of the plate, with increasing elastic spring constant, has been established; with closed-form coefficients of the waveforms (cosine, sine, cosh, sinh). Merely the rigid-body frequency parameter is insufficient in determining the prominence of the corresponding modes.
- ***Demonstrating a complete set of admissible functions for FFFF plate*** (i.e. combination of present rigid body modes with polynomial functions and trigonometric functions).

2. Analysis

2.1. Euler-Bernoulli beam vibration: generation of admissible functions

The governing differential equation of free vibration of a uniform, homogenous Euler Bernoulli beam is:

$$m\frac{\partial^2 z(x,t)}{\partial t^2}+EI\frac{\partial^4 z(x,t)}{\partial x^4}=0, \tag{2.1}$$

where m is mass per unit length [kg/m], and EI is the flexural rigidity [N/m^2] against pure bending, $z(xt)$ is the transverse small-amplitude displacement. The non-classical boundary condition is modelled as a translational spring (Fig. 1a), acting transversely to the longitudinal axis of the beam. The spring constant is k_T [N/m], which is non-dimensionalized as $K_T=\frac{k_T L^3}{EI}$.

2.1.1. TT beam (beam with both ends supported by equal translational springs). The beam is subject to the elastically-supported boundary conditions:

$$\begin{aligned} &EI\frac{\partial^2 z(0,t)}{\partial x^2}=0, \qquad &&EI\frac{\partial^3 z(0,t)}{\partial x^3}=-k_T z(0,t),\\ &EI\frac{\partial^2 z(L,t)}{\partial x^2}=0, \qquad &&EI\frac{\partial^3 z(L,t)}{\partial x^3}=k_T z(L,t), \end{aligned} \tag{2.2}$$

i.e. the bending moments are zero, while the shear force balances the spring force due to the end deflection.

Noting the two extreme cases of the end spring constant:

- As $K_T\to 0$, the beam behaves like a Free-Free (FF) beam, i.e. the end shear force vanishes.
- As $K_T\to\infty$, the beam behaves as a simply supported (SS) beam, i.e. the end deflection becomes zero.

By using separation of variables on Eq. (2.1), the general solution of the mode-shape is

$$G(x)\equiv G_1\cos\beta x+G_2\sin\beta x+G_3\cosh\beta x+G_4\sinh\beta x, \tag{2.3}$$

where $\beta^4=\frac{m\omega^2}{EI}$ and $\omega=(\beta L)^2\sqrt{\frac{EI}{mL^4}}$. Here, βL is the non-dimensional parameter, ω is the frequency [rad/s], and β is the wave number [1/m]. The waveform coefficients G_1, G_2, G_3, G_4 are constants to be evaluated from the boundary conditions (Eqs. (2.2)) as follows:

$$\begin{bmatrix} -1 & 0 & 1 & 0 \\ -\cos\beta L & -\sin\beta L & \cosh\beta L & \sinh\beta L \\ \dfrac{k}{EI} & -\beta^3 & \dfrac{k}{EI} & \beta^3 \\ a^* & b^* & c^* & d^* \end{bmatrix} \begin{Bmatrix} G_1 \\ G_2 \\ G_3 \\ G_4 \end{Bmatrix} = \begin{Bmatrix} 0 \\ 0 \\ 0 \\ 0 \end{Bmatrix}, \tag{2.4}$$

where

$$a^* = \left\{ \frac{k}{EI} \cos\beta L - \beta^3 \sin\beta L \right\}, \qquad b^* = \left\{ \frac{k}{EI} \sin\beta L + \beta^3 \cos\beta L \right\},$$

$$c^* = \left\{ \frac{k}{EI} \cosh\beta L - \beta^3 \sinh\beta L \right\}, \qquad d^* = \left\{ \frac{k}{EI} \sinh\beta L - \beta^3 \cosh\beta L \right\}.$$

For a non-trivial solution, the determinant of the square matrix is zero. The frequency expression becomes:

$$\begin{aligned} f(\beta L) = 2(\beta L)^6 (\cos\beta L \cosh\beta L - 1) - 4K_T^2 \sin\beta L \sinh\beta L \\ - 4(\beta L)^3 K_T (\cos\beta L \sinh\beta L - \cosh\beta L \sin\beta L). \end{aligned} \tag{2.5}$$

Thus, $f(\beta L) = 0$ gives the distinct frequency parameters βL for a given K_T.

- As $K_T \to 0$, Eq. (2.5) becomes $\cos\beta L \cosh\beta L = 1$, the classical frequency equation for a free-free beam. Also, $\frac{\mathrm{d} f(\beta L)}{\mathrm{d}(\beta L)} = 0$; $\frac{\mathrm{d}^2 f(\beta L)}{\mathrm{d}(\beta L)^2} \to 0$, causing the second frequency parameter to coincide with the first at $\beta L = 0$.
- As $K_T \to \infty$, it becomes $\sin\beta L \sinh\beta L = 0$, the classical frequency equation of a simply-supported beam. Since $\sinh\beta L \neq 0$ for $\beta L \neq 0$, the frequency equation becomes $\sin\beta L = 0$. Also, $\frac{\mathrm{d} f(\beta L)}{\mathrm{d}(\beta L)} = 0$; $\frac{\mathrm{d}^2 f(\beta L)}{\mathrm{d}(\beta L)^2} \to \infty$, causing the 2nd frequency parameter to become $\beta L = \pi$. From the system of equations in Eq. (2.4)

(2.6)

$$G_2 = 1, \qquad \frac{G_4}{G_2} = \frac{-2\,(K_{TL}) \sin\beta L + (\beta L)^3 (\cosh\beta L - \cos\beta L)}{-2\,(K_{TL}) \sinh\beta L + (\beta L)^3 (\cosh\beta L - \cos\beta L)},$$

$$\frac{G_1}{G_2} = \frac{-\big(K_{TR} \sin\beta L + (\beta L)^3 \cos\beta L\big) + \big\{-K_{TR} \sinh\beta L) + (\beta L)^3 \cosh\beta L\big\} \frac{G_4}{G_2}}{K_{TR} (\cos\beta L + \cosh\beta L) - (\beta L)^3 (\sinh\beta L + \sin\beta L)},$$

$$G_3 = G_1,$$

where $K_{TL} = K_T$ on the left hand side $x = 0$, $K_{TR} = K_T$ on the right hand side $x = L$.

- As $K_T \to 0$, $\beta L \to 0$, $G_2 = 1$; $\frac{G_4}{G_2} = 1$, $\frac{G_1}{G_2} = \frac{-\cos\beta L + \cosh\beta L}{-\sin\beta L - \sinh\beta L} \to \frac{0}{0}$ form!; $G_3 = G_1$. For the classical FF beam, two waveform coefficients, i.e. G_1 and G_3, are undefined, and hence Eq. (2.6) is not applicable to define the rigid-body modeshape. An alternative attempt to define the modeshape has been made in Subsec. 2.2.1.
- As $K_T \to \infty$, $G_2 = 1$, $\frac{G_4}{G_2} = \frac{\sin\beta L}{\sinh\beta L}$, $\frac{G_1}{G_2} = 0$, $G_3 = G_1$, since $\beta L \to n\pi$, $n = 1, 2, 3, \ldots$, $\frac{G_4}{G_2} \to 0$. Thus, only the coefficient G_2 dominates at this classical end condition and a sinusoidal modeshape is obtained.

2.1.2. ST beam (beam with left side hinged and right side elastically supported). Now we consider a similar beam that is hinged on the left and translationally restrained at the right (Fig. 1b), which is again modelled as a translational spring. The beam is subject to the boundary conditions:

$$\begin{aligned} &z(0,t) = 0, && EI\frac{\partial^2 z(0,t)}{\partial x^2} = 0, \\ &EI\frac{\partial^2 z(L,t)}{\partial x^2} = 0, && EI\frac{\partial^3 z(L,t)}{\partial x^3} = k_T z(L,t). \end{aligned} \tag{2.7}$$

i.e. the end bending moments are zero, the LHS deflection is zero, while the shear force at the right end balances the spring force due to the end deflection. Noting the two extreme cases:

- As $K_T \to 0$, the beam behaves like a Hinged-Free (SF) beam, i.e. the RHS shear force vanishes.
- As $K_T \to \infty$, the beam behaves as a simply supported (SS) beam, i.e. the deflection is zero at the RHS.

The constants G_1, G_2, G_3, G_4 are evaluated from the boundary conditions (Eqs. (2.7))as follows:

$$\begin{bmatrix} 1 & 0 & 1 & 0 \\ -1 & 0 & 1 & 0 \\ 0 & -\sin\beta L & 0 & \sin\beta L \\ 0 & e^* & 0 & f^* \end{bmatrix} \begin{Bmatrix} G_1 \\ G_2 \\ G_3 \\ G_4 \end{Bmatrix} = \begin{Bmatrix} 0 \\ 0 \\ 0 \\ 0 \end{Bmatrix}, \tag{2.8}$$

where

$$e^* = \left\{\frac{k}{EI}\sin\beta L + \beta^3\cos\beta L\right\}, \qquad f^* = \left\{\frac{k}{EI}\sinh\beta L - \beta^3\cosh\beta L\right\}.$$

For a non-trivial solution, the determinant of the square matrix is zero. The frequency expression becomes:

$$f(\beta L) = 2(\beta L)^3(\cos\beta L \sinh\beta L - \sin\beta L\cosh\beta L) + 4K_T \sin\beta L \sinh\beta L. \tag{2.9}$$

Thus, $f(\beta L)=0$ gives the distinct frequency parameters βL for a given K_T.

- As $K_T \to 0$, Eq. (2.9) becomes $\tan\beta L = \tanh\beta L$, which is the classical frequency equation for a SF beam. Also, $\frac{\mathrm{d}f(\beta L)}{\mathrm{d}(\beta L)} = 0$, $\frac{\mathrm{d}^2 f(\beta L)}{\mathrm{d}(\beta L)^2} \to 0$, causing the second frequency parameter to coincide with the first at $\beta L = 0$.
- As $K_T \to \infty$, Eq. (2.9) becomes $\sin\beta L \sinh\beta L = 0$, the classical frequency equation of a SS beam. Also, $\frac{\mathrm{d}f(\beta L)}{\mathrm{d}(\beta L)} = 0$, $\frac{\mathrm{d}^2 f(\beta L)}{\mathrm{d}(\beta L)^2} \to \infty$, causing the second frequency parameter to become $\beta L = \pi$.

From the system of equations in Eq. (2.8),

$$G_1 = G_3 = 0, \qquad G_2 = 1,$$

$$\frac{G_4}{G_2} = \frac{K_{TR}\sin\beta L + (\beta L)^3\cos\beta L}{-K_{TR}\sinh\beta L + (\beta L)^3\cosh\beta L}, \tag{2.10}$$

where $K_{TL} = K_T$ on left hand side, $K_{TR} = K_T$ on right hand side. The modeshape switches from the rotational rigid-body mode to the first flexural mode when the sinusoidal behaviour starts dominating at the higher wave number over the hyperbolic sinusoidal behaviour, thereby causing a curvature to develop.

- As $K_{TR} \to 0$, $G_2 = 1$, $\frac{G_4}{G_2} = \frac{\cos\beta L}{\cosh\beta L} = 1$, $G_1 = G_3 = 0$. Both the sine and hyperbolic sine functions show a linear behaviour for a small wave number, and hence contribute almost equally.
- As $K_{TR} \to \infty$, $G_2 = 1$, $\frac{G_4}{G_2} \to -\frac{\sin\beta L}{\sinh\beta L}$, $G_1 = G_3 = 0$. Since $\beta L \to n\pi$, $n = 1, 2, 3, \ldots$, $\frac{G_4}{G_2} \to 0$. Thus, only the coefficient G_2 dominates at this classical end condition and a sinusoidal modeshape is obtained.

2.2. Generation of closed-form rigid-body modeshapes with classical edge condition

The flexural modes of the Euler-Bernoulli beam form an orthogonal set of functions. But for beam with trivial frequencies (rigid-body behaviour), it is necessary to generate the rigid-body modeshapes which (i) satisfy the boundary conditions, (ii) have zero curvature, and (iii) form an orthogonal set.

2.2.1. TT beam (beam with both ends translationally supported). Equation (2.5) yields two rigid body modes: translation (T) and rotation (R). The respective frequency parameters of the rigid-body modes are $\beta_T L$, $\beta_R L$, and the associated modeshapes are $\phi_T(x)$, $\phi_R(x)$. From the general solution of the modeshape in Eq. (2.3), the rigid-body modeshapes are expressed as:

$$\begin{aligned} \phi_T(x) &= T_1\cos\beta_T x + T_2\sin\beta_T x + T_3\cosh\beta_T x + T_4\sinh\beta_T x,\\ \phi_R(x) &= R_1\cos\beta_R x + R_2\sin\beta_R x + R_3\cosh\beta_R x + R_4\sinh\beta_R x, \end{aligned} \tag{2.11}$$

where the unknown waveform coefficients T_i, R_i, $i = 1, 2, 3, 4$; are calculated from the boundary conditions. Assuming the translational modeshape to be simply a transverse displacement, and the rotational modeshape to be about the longitudinal midpoint $x = \frac{L}{2}$ of the beam (Fig. 1b), the modeshapes may be expressed as:

$$\begin{aligned} \phi_T(x) &= 1 = x^0 + 0.x^1 + 0.x^2 + 0.x^3 + \cdots ; \\ \phi_R(x) &= 1 - \frac{2x}{L} = x^0 - \left(\frac{2}{L}\right) x^1 + 0.x^2 + 0.x^3 + \cdots \end{aligned} \tag{2.12}$$

Equating the coefficients of the same power of Eq. $(2.11)_1$ and Eq. $(2.12)_1$:

$$\begin{aligned} T_1 \left(1 - \frac{(\beta_T x)^2}{2!} + \frac{(\beta_T x)^4}{4!} - \cdots\right) + T_2 \left(\beta_T x - \frac{(\beta_T x)^3}{3!} + \frac{(\beta_T x)^5}{5!} - \cdots\right) \\ + T_3 \left(1 + \frac{(\beta_T x)^2}{2!} + \frac{(\beta_T x)^4}{4!} + \cdots\right) + T_4 \left(\beta_T x + \frac{(\beta_T x)^3}{3!} + \frac{(\beta_T x)^5}{5!} + \cdots\right) \\ = 1.x^0 + 0.x^1 + 0.x^2 + 0.x^3 + \cdots \end{aligned} \tag{2.13}$$

Therefore $T_1 + T_3 = 1$, $T_2 + T_4 = 0$, $-T_1 + T_3 = 0$, $-T_2 + T_4 = 0 \Rightarrow T_2 = 0$, $T_4 = 0$, $T_1 = T_3 = 0.5$.

Thus, the final translational rigid-body modeshape becomes:

$$\phi_T(x) = 0.5 \cos \beta_T x + 0.5 \cosh \beta_T x. \tag{2.14}$$

For rigid-body translation, the frequency parameter is exactly zero, irrespective of the magnitude of K_T, leading to $\phi_T(x) = 1$, satisfying Eq. $(2.12)_1$. This modeshape must have zero curvature, since it is a rigid-body modeshape. It is seen that $\frac{\mathrm{d}^2\phi_T(x)}{\mathrm{d}x^2} = \beta_T^2 (-0.5 \cos \beta_T x + 0.5 \cosh \beta_T x) = 0$ for all values of x, i.e. at all location on the beam. Similarly, equating the coefficients of the same power of Eq. $(2.11)_2$ and Eq. $(2.12)_2$:

$$\begin{aligned} R_1 \left(1 - \frac{(\beta_R x)^2}{2!} + \frac{(\beta_R x)^4}{4!} - \cdots\right) + R_2 \left(\beta_R x - \frac{(\beta_R x)^3}{3!} + \frac{(\beta_R x)^5}{5!} - \cdots\right) \\ + R_3 \left(1 + \frac{(\beta_R x)^2}{2!} + \frac{(\beta_R x)^4}{4!} + \cdots\right) + R_4 \left(\beta_R x + \frac{(\beta_R x)^3}{3!} + \frac{(\beta_R x)^5}{5!} + \cdots\right) \\ = x^0 - \left(\frac{2}{L}\right) x^1 + 0.x^2 + 0.x^3 + \cdots \end{aligned} \tag{2.15}$$

Therefore, $R_1 + R_3 = 1$, $R_2 + R_4 = -\frac{2}{\beta L}$, $-R_1 + R_3 = 0$, $-R_2 + R_4 = 0 \Rightarrow$ $R_1 = R_3 = 0.5$, $R_2 = R_4 = -\frac{1}{\beta L}$.

Thus, the final rotational rigid-body modeshape becomes:

$$\phi_R(x) = 0.5\cos\beta_R x - \frac{1}{\beta_R L}\sin\beta_R x + 0.5\cosh\beta_R x - \frac{1}{\beta_R L}\sinh\beta_R x. \tag{2.16}$$

For the rotational rigid-body modeshapes, the frequency parameter $\beta_R L \neq 0$. It is seen that $\phi_T(x)$ and $\phi_R(x)$ are orthogonal to each other. This modeshape must have zero curvature, since it is a rigid-body modeshape.

It is seen that

$$\frac{\mathrm{d}^2\phi_R(x)}{\mathrm{d}x^2} = \beta_R^2\left(-0.5\cos\beta_R x + \frac{1}{\beta_R L}\sin\beta_R x + 0.5\cosh\beta_R x - \frac{1}{\beta_R L}\sinh\beta_R x\right)$$

is negligibly small. Expanding the curvature expression as a Taylor's series:

$$\phi_R''(x) = \beta_R^2\begin{bmatrix} -0.5\left(1 - \frac{(\beta_R x)^2}{2!} + \frac{(\beta_R x)^4}{4!} - \ldots\right) + \frac{1}{\beta_R L}\left(\beta_R x - \frac{(\beta_R x)^3}{3!} + \frac{(\beta_R x)^5}{5!} - \ldots\right) \\ +0.5\left(1 + \frac{(\beta_R x)^2}{2!} + \frac{(\beta_R x)^4}{4!} + \ldots\right) - \frac{1}{\beta_R L}\left(\beta_R x + \frac{(\beta_R x)^3}{3!} + \frac{(\beta_R x)^5}{5!} + \ldots\right)\end{bmatrix}$$
$$= O\left((\beta_R x)^4\right) + O\left((\beta_R x)^8\right).$$

For a tolerance $|\phi_R''(x)| \leq 10^{-8}$, the frequency parameter $\beta_R L \leq 10^{-2}$, i.e. this modeshape is valid for a very small frequency parameters, which does not store potential energy but participates in the kinetic energy.

2.2.2. Hinged-Free (SF) beam. This beam has one rigid-body mode, i.e. the rotational rigid-body mode. Assuming the rotation to be about the left end of the beam, the linear modeshape may be expressed as:

$$\phi_R(x) = \frac{x}{L} = 0.x^0 + \left(\frac{1}{L}\right)x^1 + 0.x^2 + 0.x^3 + \cdots \tag{2.17}$$

Equating the coefficients of the same power of Eq. $(2.11)_2$ and Eq. (2.17):

$$R_1\left(1 - \frac{(\beta_R x)^2}{2!} + \frac{(\beta_R x)^4}{4!} - \cdots\right) + R_2\left(\beta_R x - \frac{(\beta_R x)^3}{3!} + \frac{(\beta_R x)^5}{5!} - \cdots\right)$$
$$+ R_3\left(1 + \frac{(\beta_R x)^2}{2!} + \frac{(\beta_R x)^4}{4!} + \cdots\right) + R_4\left(\beta_R x + \frac{(\beta_R x)^3}{3!} + \frac{(\beta_R x)^5}{5!} + \cdots\right)$$
$$= 0.x^0 + \left(\frac{1}{L}\right)x^1 + 0.x^2 + 0.x^3 + \ldots. \tag{2.18}$$

Therefore, $R_1 + R_3 = 0$, $R_2 + R_4 = \frac{1}{\beta L}$, $-R_1 + R_3 = 0$, $-R_2 + R_4 = 0 \Rightarrow R_1 = R_3 = 0$, $R_2 = R_4 = \frac{1}{2\beta L}$.

Thus, the final rotational rigid-body modeshape becomes:

$$\phi_R(x) = \frac{1}{2\beta_R L}\sin\beta_R x + \frac{1}{2\beta_R L}\sinh\beta_R x. \tag{2.19}$$

For the rotational rigid-body modeshapes, the frequency parameter $\beta_R L \neq 0$. This modeshape must again have zero curvature. It is seen that its curvature, which is the second derivative of Eq. (2.19), i.e.

$$\frac{\mathrm{d}^2\phi_R(x)}{\mathrm{d}x^2} = \beta_R^2\left(-\frac{1}{2\beta_R L}\sin\beta_R x + \frac{1}{2\beta_R L}\sinh\beta_R x\right)$$

is negligibly small. Expanding its expression as a Taylor's series:

$$\phi_R''(x) = \frac{\beta_R^2}{2\beta_R L}\left[-\left(\beta_R x - \frac{(\beta_R x)^3}{3!} + \frac{(\beta_R x)^5}{5!} - \dots\right)\right. \\ \left. + \left(\beta_R x + \frac{(\beta_R x)^3}{3!} + \frac{(\beta_R x)^5}{5!} + \dots\right)\right] = O\left((\beta_R x)^4\right) + O\left((\beta_R x)^8\right).$$

For a tolerance $|\phi_R''(x)| \leq 10^{-8}$, the frequency parameter $\beta_R L \leq 10^{-2}$ i.e. this modeshape is valid for a very small frequency parameters, which does not store potential energy but participates in the kinetic energy.

2.3. Kirchhoff's plate vibration: elastically supported edges

Once the rigid-body modeshapes and the flexural modeshapes of the TT and ST beams are available as explained in Subsec. 2.2, they can be used as beam-wise admissible functions in the Rayleigh-Ritz method to analyse the vibration of plates with several boundary conditions: TTTT, STTT, SSTT, STST, and SSST plates. As $K_T \to 0$, we get plates like FFFF, SFFF, SSFF, SFSF, and SSSF. As $K_T \to \infty$, we get the SSSS plate. The linear, second-order, homogeneous, governing differential equation (GDE) for the free vibration of an isotropic Kirchhoff's plate, ignoring gravity, is given below. The transverse out-of-plane small-amplitude vibratory displacement $Z(x, y, t)$ satisfies the partial differential equation

$$m_p\ddot{Z}(x, y, t) + D\nabla^4 Z(x, y, t) = 0. \tag{2.20}$$

Here, m_p is the mass per unit area of the plate and $D = \frac{Eh^3}{12(1-\nu^2)}$ is the flexural rigidity of the isotropic plate. The plate in Fig. 1c is subject to the coupled boundary conditions as shown in Warburton and Edney [25]:

- The bending moments are zero at the ends, i.e.

$$\frac{\partial^2 Z(0,y,t)}{\partial x^2}+\nu\frac{\partial^2 Z(0,y,t)}{\partial y^2}=0,\qquad \frac{\partial^2 Z(L,y,t)}{\partial x^2}+\nu\frac{\partial^2 Z(L,y,t)}{\partial y^2}=0,$$

$$\frac{\partial^2 Z(x,0,t)}{\partial y^2}+\nu\frac{\partial^2 Z(x,0,t)}{\partial x^2}=0,\qquad \frac{\partial^2 Z(x,L,t)}{\partial y^2}+\nu\frac{\partial^2 Z(x,L,t)}{\partial x^2}=0.$$

- The shear force at the edges equals the spring force produced due to the deflection of the modeshape, i.e.

$$EI\frac{\partial^3 Z(0,y,t)}{\partial x^3}+(2-\nu)\frac{\partial^3 Z(0,y,t)}{\partial x\partial y^2}=k_{t0x}Z(0,y,t),$$

$$EI\frac{\partial^3 Z(L,y,t)}{\partial x^3}+(2-\nu)\frac{\partial^3 Z(L,y,t)}{\partial x\partial y^2}=k_{t1x}Z(L,y,t),$$

$$EI\frac{\partial^3 Z(x,0,t)}{\partial y^3}+(2-\nu)\frac{\partial^3 Z(x,0,t)}{\partial y\partial x^2}=k_{t0y}Z(x,0,t),$$

$$EI\frac{\partial^3 Z(x,L,t)}{\partial y^3}+(2-\nu)\frac{\partial^3 Z(x,L,t)}{\partial y\partial x^2}=k_{t1y}Z(x,L,t).$$

Simplifying the relations to avoid the coupling, the BCs have been approximated as given by Zhou [27]

$$\begin{aligned}&\frac{\partial^2 Z(0,y,t)}{\partial x^2}=0, &&\frac{\partial^2 Z(L,y,t)}{\partial x^2}=0,\\ &\frac{\partial^2 Z(x,0,t)}{\partial y^2}=0, &&\frac{\partial^2 Z(x,L,t)}{\partial y^2}=0,\end{aligned}\tag{2.21}$$

$$\begin{aligned}&EI\frac{\partial^3 Z(0,y,t)}{\partial x^3}=k_{t0x}Z(0,y,t), &&EI\frac{\partial^3 Z(L,y,t)}{\partial x^3}=k_{t1x}Z(L,y,t),\\ &EI\frac{\partial^3 Z(x,0,t)}{\partial y^3}=k_{t0y}Z(x,0,t), &&EI\frac{\partial^3 Z(x,L,t)}{\partial y^3}=k_{t1y}Z(x,L,t).\end{aligned}\tag{2.22}$$

Assuming, $Z(x,y,t)=W(x,y)\,e^{i\omega t}$, where $W(x,y)$ is the spatial shape, $\xi=\frac{x}{a}$, $\eta=\frac{y}{b}$, and $\lambda=\frac{a}{b}=$ aspect ratio, the maximum strain energy stored in a plate is

$$(2.23)\quad U_{\max(\text{plate})} = \frac{D}{2}\frac{b}{a^3}\int_0^1\int_0^1\Bigg[\left(\frac{\partial^2 W}{\partial \xi^2}\right)^2 + \left(\frac{a}{b}\right)^4\left(\frac{\partial^2 W}{\partial \eta^2}\right)^2 + 2\nu\left(\frac{a}{b}\right)^2\frac{\partial^2 W}{\partial \xi^2}\frac{\partial^2 W}{\partial \eta^2} + 2\,(1-\nu)\left(\frac{a}{b}\right)^2\left(\frac{\partial^2 W}{\partial \xi \partial \eta}\right)^2\Bigg]\,\mathrm{d}\xi\,\mathrm{d}\eta.$$

The maximum strain energy stored in a translational spring

$$(2.24)\quad U_{\max(\text{spring})} = \frac{1}{2}k_{t0x}b\int_0^1 \left(W^2\right)_{\xi=0}\,\mathrm{d}\eta + \frac{1}{2}k_{t1x}b\int_0^1 \left(W^2\right)_{\xi=1}\,\mathrm{d}\eta + \frac{1}{2}k_{t0y}a\int_0^1 \left(W^2\right)_{\eta=0}\,\mathrm{d}\xi + \frac{1}{2}k_{t1y}a\int_0^1 \left(W^2\right)_{\eta=1}\,\mathrm{d}\xi.$$

The maximum kinetic energy of the plate

$$(2.25)\quad T_{\max(\text{plate})} = \frac{1}{2}\rho h\omega^2 ab\int_0^1\int_0^1 W^2\,\mathrm{d}\xi\,\mathrm{d}\eta.$$

The energy-based Rayleigh-Ritz Method is used to minimize the difference between potential energy and kinetic energy with respect to the unknown coefficient. Let $W(x, y)$ be a weighted combination of the product of the beam modeshapes in either direction as follows:

$$(2.26)\quad W(\xi,\eta) = \sum_{i=1}^{\infty}\sum_{j=1}^{\infty} C_{ij}\phi_i(\xi)\,\phi_j(\eta).$$

Minimizing the plate natural frequency with respect to each of the unknown coefficients

$$(2.27)\quad \left(\frac{\partial}{\partial C_{ij}}\right)\left[U_{\max(\text{plate})} + U_{\max(\text{spring})} - T_{\max(\text{plate})}\right] = 0$$

leads to the eigen value problem

$$(2.28)\quad \big([K] - \Omega^2[M]\big)\{C\} = 0$$

with $\Omega^2 = \frac{\rho h\omega^2 a^4}{D}$ is the non-dimensional frequency and ω^2 is the dimensional frequency [rad/s]. Here,

$$K_{ijkp(\text{plate})} = A_{ik}^{(2,2)}B_{jp}^{(0,0)} + \left(A_{ik}^{(0,0)}B_{jp}^{(2,2)}\right)\lambda^4 + \nu\left(A_{ik}^{(0,2)}B_{jp}^{(2,0)} + A_{ik}^{(2,0)}B_{jp}^{(0,2)}\right)\lambda^2 + 2\,(1-\nu)\,A_{ik}^{(1,1)}B_{jp}^{(1,1)}\lambda^2,$$

$$K_{ijkp(\text{spring})} = K_{T1}\phi_i(0)\,\phi_k(0)\,B_{jp}^{(0,0)} + K_{T3}\phi_i(1)\,\phi_k(1)\,B_{jp}^{(0,0)} + \lambda^4 K_{T4}\phi_j(0)\,\phi_p(0)\,A_{ik}^{(0,0)} + \lambda^4 K_{T2}\phi_j(1)\,\phi_p(1)\,A_{ik}^{(0,0)},$$

where

$$K_{T1} = \frac{k_{t0x}a^3}{D}, \qquad K_{T3} = \frac{k_{t1x}a^3}{D}, \qquad K_{T4} = \frac{k_{t0y}b^3}{D},$$

$$K_{T2} = \frac{k_{t1y}b^3}{D}, \qquad M_{ijkp} = A_{ik}^{(0,0)}B_{jp}^{(0,0)},$$

$$A_{i,k}^{m,n} = \int_0^1 \frac{d^m\phi_i(\xi)}{d\xi^m}\frac{d^n\phi_k(\xi)}{d\xi^n}\,\mathrm{d}\xi, \qquad B_{j,p}^{m,n} = \int_0^1 \frac{d^m\phi_j(\eta)}{d\eta^m}\frac{d^n\phi_p(\eta)}{d\eta^n}\,\mathrm{d}\eta,$$

where $m,n = 0,1,2,\ i,k,j,p = 1,2,3,\ldots$.

Analytical integration of Eqs. (2.23)–(2.25) has been done for higher accuracy. Along with this, the availability of orthogonal beam modeshapes (including rigid-body modes) causes the stiffness matrix to be more diagonally dominant, leading to higher computational efficiency, since less number of terms in Eq. (2.26) are required to converge to the plate natural frequency.

3. Results

In this section, we first discuss the results of the beam frequency parameters for changing translation edge restraints, and the corresponding beam modeshapes. The prominence of the rigid-body modeshapes is included. Then the natural frequencies of non-classically supported plates are presented, for various permutations and combinations of edge restraints. The convergence of the frequencies of the classical conditions is shown versus the number of admissible functions in the Rayleigh-Ritz method. The first few modeshapes of the FFFF plate are also presented.

3.1. TT beam

Figure 2 shows the frequency expression of the above elastically end supported beam vs. the frequency parameter, for a large range of the translational spring constant K_T. The frequency expression characteristic starts from zero irrespective of the spring constant K_T. The slope of the characteristics is also zero for all K_T at $\beta L = 0$. However, the curvature of the characteristics is positive for all $K_T > 0$ at $\beta L = 0$. The characteristic rises from $\beta L = 0$ and descends to the X-axis to give the frequency parameter for the rotational rigid-body mode, for $K_T < \infty$. The next band-width of frequency parameters is $4.73 < \beta L < 2\pi$

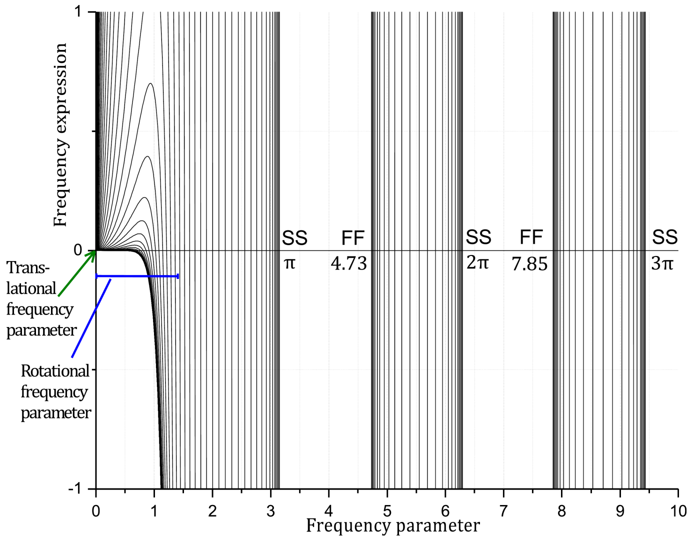

FIG. 2. Frequency expression of a beam with translational edge support at both ends (TT beam) vs. frequency parameter.

starting with the first flexural mode of the FF beam and approaching the second flexural mode of the SS beam.

Figure 3 shows the frequency parameters of an Euler-Bernoulli beam with both ends non-classically supported by equal translational restraints, vs. the

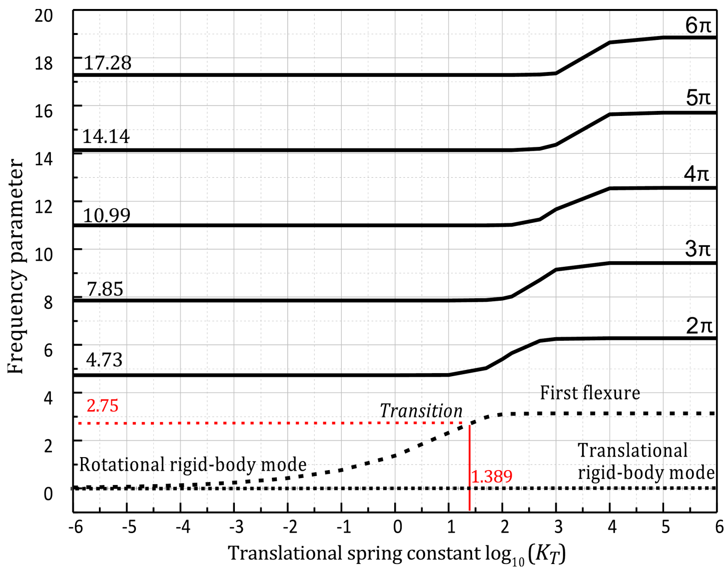

FIG. 3. TT Beam frequency parameter as a function of translational end spring constants.

translational spring constant K_T. The trivial solution $\beta L = 0$ is valid for all values of K_T. There is a transition from the free-free beam to the simply-supported beam behaviour at a particular zone of K_T; but the zone is different for different modes. The transition zone shifts to a higher magnitude of K_T for the higher-order modes. When $K_T \approx 0$, there are two coincident rigid-body frequency parameters $\beta L = 0$. As $K_T > 0$, this characteristic bifurcates into two, one remaining at $\beta L = 0$, leading to the translational rigid-body mode, while the other reaching $\beta L \leq \pi$, switching from the rotational rigid-body mode to the first flexural mode at $\beta L = \pi$.

The rigid-body frequency parameters precipitate from the frequency equation, but the prominence of the rigid-body modes depend on K_T. The larger the spring constant, the feebler is the rigid-body mode contribution to the vibration. As $K_T \to \infty$, the rigid-body modeshapes vanish. As $K_T \to 0$, the rigid-body modeshape become prominent. This prominence cannot be known from the frequency equation alone. They must be known from the solution set of the four boundary conditions, i.e. the coefficients of Eq. (2.3).

Table 1 shows the coefficients of the waveforms of the rigid-body modeshapes of the TT beam. Since the frequency parameter of the translational modeshape is zero, the values of T_2 and T_4 are irrelevant in the final modeshape, and the values of T_1 and T_3 simply sum up to give the amplitude of the translational mode. As the edge spring constant K_T increases, the total amplitude of the

Table 1. Coefficients of waveforms of translational and rotational rigid-body modeshape of TT beam.

$\log_{10}(K_T)$	T_1	T_2	T_3	T_4	T_1+T_3	R_1	R_2	R_3	R_4
−6	−1.0000	0.0000	0.0000	0.0000	**1.0000**	0.0175	−0.7067	0.0175	−0.7070
−5	−1.0000	0.0000	0.0000	0.0000	**1.0000**	0.0311	−0.7060	0.0311	−0.7069
−4	−1.0000	0.0000	0.0001	−0.0001	**0.9999**	0.0552	−0.7035	0.0552	−0.7064
−3	−1.0000	0.0000	0.0010	−0.0010	**0.9990**	0.0975	−0.6958	0.0975	−0.7049
−2	0.9999	0.0000	−0.0098	0.0098	**0.9901**	0.1698	−0.6723	0.1698	−0.7003
−1	0.9929	0.0000	−0.0838	0.0838	**0.9091**	0.2845	−0.6043	0.2845	−0.6877
0	0.8629	0.0000	−0.3574	0.3574	**0.5054**	0.4323	−0.4351	0.4323	−0.6610
1	0.6421	0.0000	−0.5421	0.5421	**0.1000**	0.5486	−0.1041	0.5486	−0.6222
						transition			
2	0.5849	0.0000	−0.5735	0.5735	**0.0114**	0.1300	0.9761	0.1300	−0.1161
3	0.5781	0.0000	−0.5770	0.5770	**0.0012**	0.0153	0.9997	0.0153	−0.0140
4	0.5774	0.0000	−0.5773	0.5773	**0.0001**	0.0015	1.0000	0.0015	−0.0014
5	0.5774	0.0000	−0.5773	0.5773	**0.0000**	0.0002	1.0000	0.0002	−0.0001
6	0.5774	0.0000	−0.5773	0.5773	**0.0000**	0.0000	1.0000	0.0000	0.0000

modeshape $T_1 + T_3$ reduces to zero. This decreasing prominence of the rigid-body mode again seen in the coefficients of the rotational rigid-body mode of the TT beam. At very low edge spring constants, the modeshape will be anti-symmetric about the midpoint of the beam (a node is present roughly at the midpoint); and large deflection at the ends; while at very high spring constants, the modeshape will be symmetric about the midpoint (approaching the first flexural mode of the SS beam) with little or no deflection at the ends.

1. At low K_T, when the rigid-body rotational mode should be prominent, the cosine and hyperbolic cosine shapes cancel out each other, and hence their coefficients R_1 and R_3 are equal. The sine and hyperbolic sine shapes reinforce each other, and hence their coefficients R_2 and R_4 are also equal, leading to the straight line shape of the rigid-body mode. The node at $x = \frac{L}{2}$ is assured by the non-zero sum of the cosine and hyperbolic cosine shape, for $K_T \leq 10^{-7}$. Increasing the K_T (and hence the wave number) leads to the node shifting away from $x = \frac{L}{2}$ for non-classical edges.
2. As K_T increases, the wavelengths of the vibration modeshapes decrease with increasing elastic support at the edges. The hyperbolic functions tend to bring in more asymmetry in the modeshape, and hence to avoid that, their coefficients R_3 and R_4 reduce to zero with increasing spring constant. As $K_T \to \infty$, both the ends tend to get more and more fixed, which is a shape satisfied only by the sine waveform function, and hence R_2 remains, with the other coefficients going to zero.

The study of the waveform coefficients G_1, G_2, G_3, G_4 normalized by G_2 (which is the coefficient of the sinusoidal waveform) from Eq. (2.6) gives the exact frequency parameter and spring constant, at which one or more of the other coefficients vanish(es), thereby demarcating the transition point. At $\log_{10}(K_T) = 1.389$ with $\beta L = 2.75$, where the two waveform coefficients G_1, G_3 are undefined; the modeshape behaviour switches from the rigid-body mode to the flexural mode. The node at $x = L/2$ suddenly vanishes off, and an antinode appears there. This sudden change requires a sudden "jump" in the anti-symmetric waveform coefficients, i.e. the cosine function. Figure 4 shows the TT beam modeshape associated with the first non-trivial frequency parameter, corresponding to the dashed-line characteristic in Fig. 3.

3.2. ST beam

Figure 5 shows the frequency expression of the above elastically end supported beam vs. the frequency parameter, for a large range of the translational spring constant K_T. The frequency expression characteristic starts from zero irrespective of the spring constant K_T The slope of the characteristics is also zero for all K_T at $\beta L = 0$. However, the curvature of the characteristics is positive

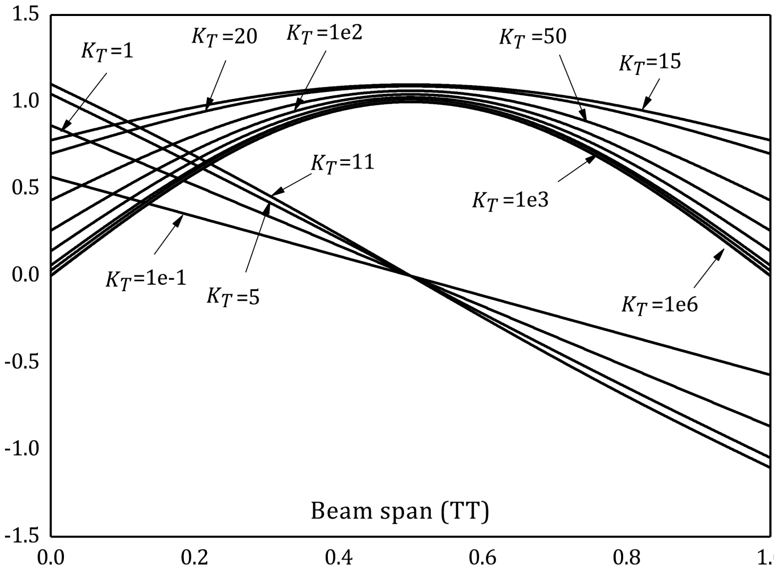

FIG. 4. Modeshape associated with the 2nd frequency parameter of TT beam: transition from rotational rigid-body modeshape of FF beam to first flexural modeshape SS beam.

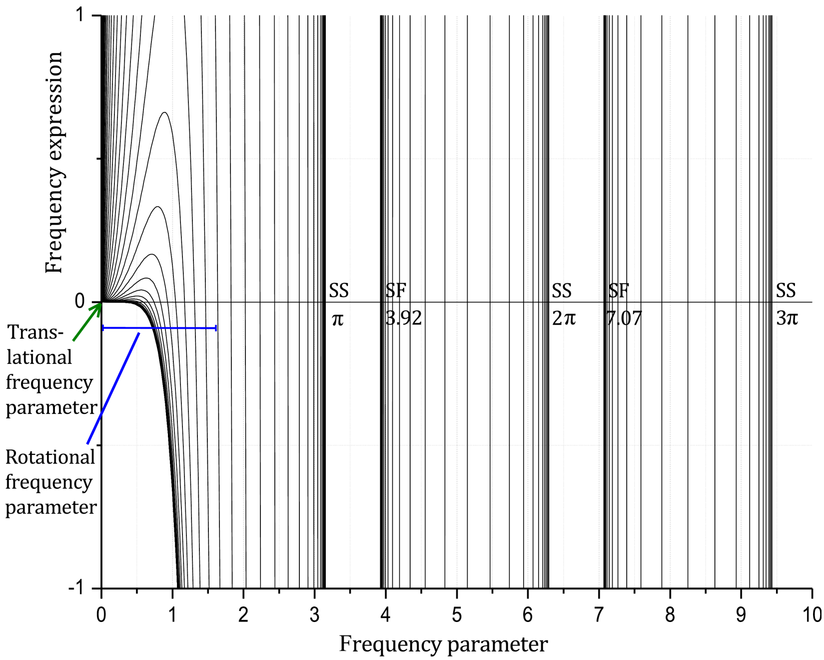

FIG. 5. Frequency expression of a beam with translational edge support at one end (ST beam) vs. frequency parameter.

for all K_T at $\beta L = 0$. The characteristic rises from $\beta L = 0$ and descends to the X-axis to give the frequency parameter for the rotational rigid-body mode, for $K_T < \infty$. The next band-width of frequency parameters is $3.92 < \beta L < 2\pi$ starting with the first flexural mode of the SF beam and approaching the second flexural mode of the SS beam.

Figure 6 shows the frequency parameters of an Euler-Bernoulli beam with one end non-classically supported by translational restraints and the other end hinged; vs. the translational spring constant K_T. The trivial solution $\beta L = 0$ is valid for all values of K_T. The rigid body mode will exist for all $K_T < \infty$. There is a transition from the hinged-free beam to the simply-supported beam behaviour at a particular zone of K_T. The transition zone shifts to higher K_T for the higher-order modes. When $K_T \approx 0$, there is the rotational rigid-body frequency parameter $\beta L = 0$. As $K_T > 0$, this characteristic approaches the first flexural mode of an SS beam, for $\beta L \leq \pi$. Table 2 shows the coefficients of the waveforms of the rigid-body modeshapes of the ST beam. Since the displacement at the left end zero, and thus the cosine and hyperbolic cosine terms should not contribute. Thus, their coefficients R_1 and R_3 are always zero.

- At low K_T, when the rigid-body mode is prominent, the sine and the hyperbolic sine functions contribute to the straight-line modeshape, with a very small wave number and hence a very large wavelength.

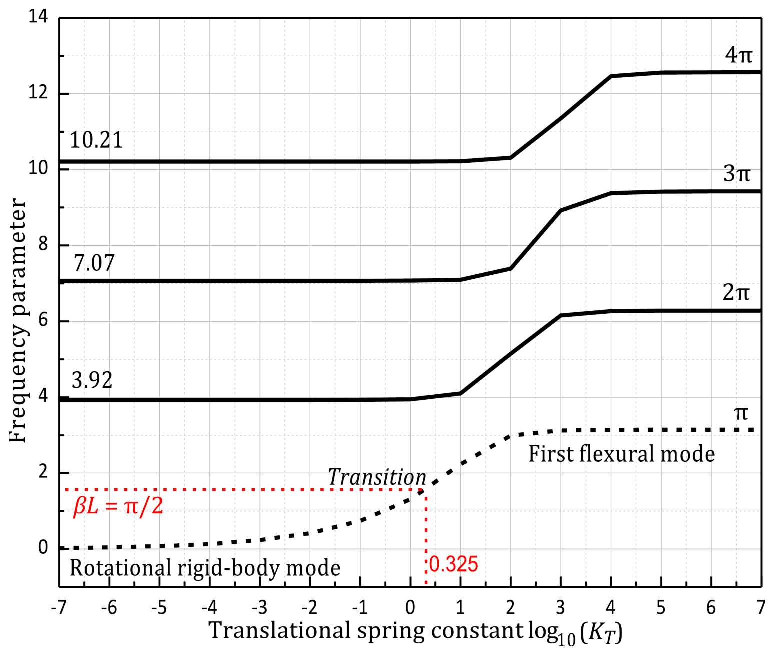

FIG. 6. ST Beam frequency parameter as a function of translational end spring constants.

- As K_T increases, and the beam tend to behave like a simply-supported beam, the shape approaches a sinusoidal form, thereby manifesting with a large R_2. The contribution of the hyperbolic sine, i.e., R_4 steadily decreases, since the right end of the beam gets more and more constrained against translation. As $K_T \to \infty$, both the ends tend to get more and more fixed, which is a shape satisfied only by the sine waveform function, and hence R_2 remains, with the other coefficients going to zero.
- In the range $10^0 < K_T < 10^1$, the rigid-body mode switches gradually to the flexural (sine) modeshape.

Table 2. Waveform coefficients of rigid-body mode (ST beam).

$\log_{10}(K_T)$	R_1	R_2	R_3	R_4
−6	0.00000	0.70731	0.00000	0.70690
−5	0.00000	0.99999	0.00000	0.00548
−4	0.00000	0.99985	0.00000	0.01732
−3	0.00000	0.99850	0.00000	0.05469
−2	0.00000	0.98535	0.00000	0.17054
−1	0.00000	0.87860	0.00000	0.47756
0	0.48687	0.69079	0.48687	0.22073
transition				
1	−0.17236	−0.96464	−0.17236	0.10027
2	0.00000	−0.99988	0.00000	−0.01538
3	0.00000	−1.00000	0.00000	−0.00136
4	0.00000	−1.00000	0.00000	−0.00013
5	0.00000	−1.00000	0.00000	−0.00001
6	0.00000	−1.00000	0.00000	0.00000

The study of the waveform coefficients G_1, G_2, G_3, G_4 normalized by G_2 (which is the coefficient of the sinusoidal waveform) from Eqs. (2.10) gives the exact frequency parameter and spring constant. For the ST beam, at roughly around $\log_{10}(K_T) = 0.325$ and correspondingly, $\beta L = \frac{\pi}{2}$, the modeshape behaviour gradually transits from the rigid-body mode to the flexural mode. Since there is nowhere that the waveform coefficients become undefined, there is no "sudden" switch in the behaviour, unlike a TT beam. The competing behaviour of the sine and the hyperbolic sine functions at higher frequency parameters slowly brings in a non-negligible curvature in the modeshape. Figure 7 shows the ST beam modeshape associated with the first non-trivial frequency parameter, corresponding to the rotational rigid-body mode characteristics in Fig. 6.

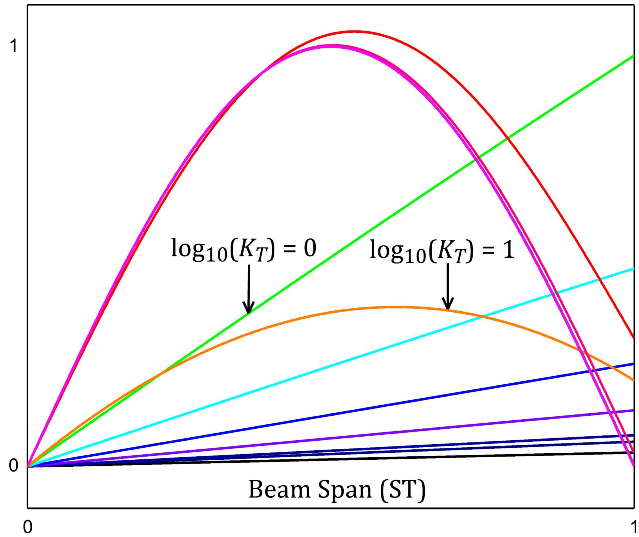

FIG. 7. Modeshape associated with the 1st frequency parameter of ST beam.

3.3. Kirchhoff's plate vibration

Figure 8 shows the first four (4) frequency parameters of a square plate with all four edges constrained against translation, vs. the translational spring constant. As the spring constant increases, the characteristics asymptote to the

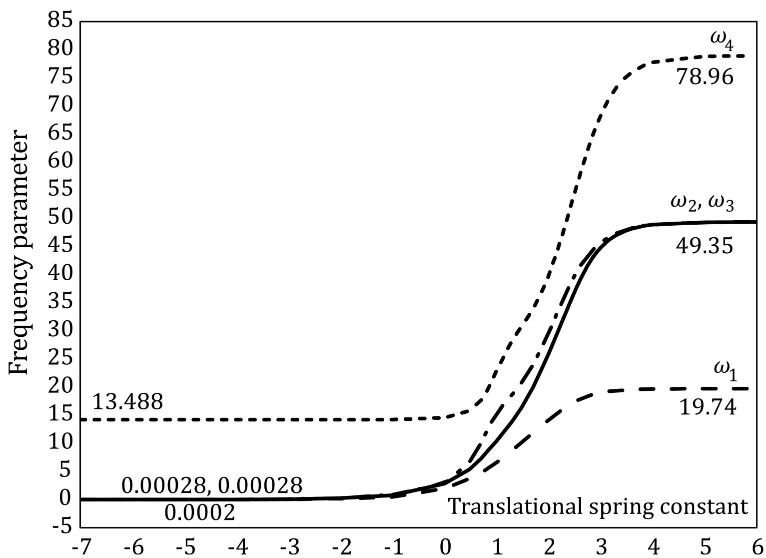

FIG. 8. Square TTTT Plate: frequency parameter as a function of translational end spring constants.

corresponding frequencies of a SSSS plate. Figure 9 shows the first four (4) frequency parameters of a square plate with three edges constrained against translation and one edge simply-supported (SFFF), vs. the translational spring constant. As the spring constant increases, the characteristics asymptote to the corresponding frequencies of a SSSS plate. The trivial frequency corresponds to the domination of the translational rigid-body mode of the FF beam and the rotational rigid-body mode from the SF beam. The second frequency (6.648) corresponds to the translational rigid-body mode of the FF beam and the first flexural mode from the SF beam. The third frequency (15.023) corresponds to the rotational rigid-body mode of the FF beam and the rotational rigid-body mode from the SF beam. The fourth frequency (25.492) corresponds to the rotational rigid-body mode of the FF beam and the first flexural mode from the SF beam. All the three non-trivial frequencies at $K_T = 10^{-7}$ have been verified with Leissa [12].

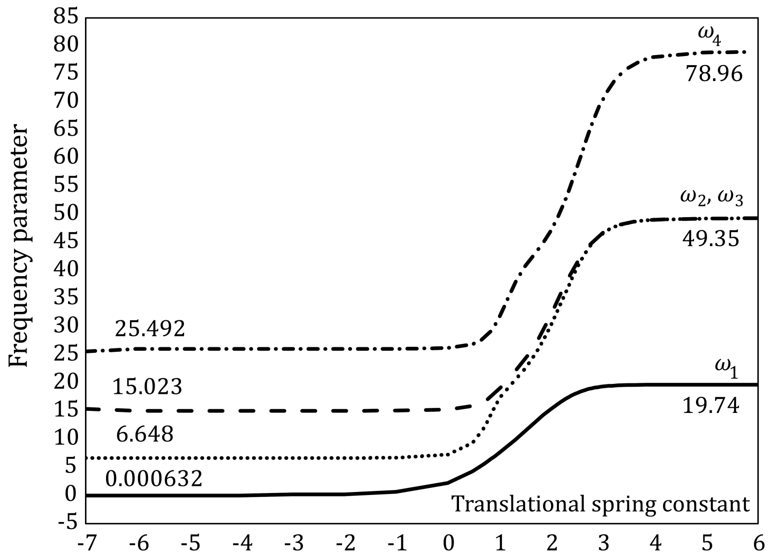

Fig. 9. Square STTT Plate: frequency parameter as a function of translational end spring constants.

It is interesting to note that the FF beam and a CC beam have the same flexural frequency parameters. Thus a CCCC plate and a FFFF plate must also have the same non-D frequencies, starting with 35.99 [12]. However, the presence of the beam-wise rigid-body modes from either direction causes the manifestation of the lower frequencies of the FFFF plate, as seen in Table 3, verified with Leissa [12], who had reported only the first six (6) frequencies.

Here we report a few more higher-frequencies. The rigid-body modes have no strain potential energy since there is no curvature. The TTTT plate has three (3) trivial frequencies, associated with its rigid-body modes, i.e. translation and rotation about its two planar axes. Theoretically, these frequencies should be zero as $K_T = 0$; however, since we use $K_T = 10^{-7}$, we get a slight non-zero value of the trivial frequency due to the potential energy stored in the spring. The value 0.0002 corresponds to the dominance of the translational rigid-body beam modeshape from either side. The value 0.00028 corresponds to the domination of the product of the translational rigid-body beam modeshape from one side and the rotational rigid-body beam modeshape from the other side. As the spring constant is increased, the trivial frequency characteristic of a TTTT plate bifurcates to the first natural frequency of the SSSS plate, i.e. 19.74, and the second/third natural frequency, i.e. 49.35, which is repeated frequency. From the 4th frequency onwards, there is a flexural beam-mode contribution from at least one side of the plate. Here, the Rayleigh-Ritz method uses 6×6 beam modes from either side as admissible functions, and the output frequencies converge to those given by Leissa [12]. The transition from the FFFF behaviour to the SSSS plate frequencies occurs at $10^1 < K_T < 10^2$, similar to the TT beam frequency characteristics in Fig. 3.

Table 4 shows the frequency convergence study of the SFFF plate, which has one rigid-body mode (rotational about the S-edge), with a trivial frequency. Here again, the Rayleigh-Ritz method uses 6×6 beam modes from either side as admissible functions, and the output frequencies converge to those given by Leissa [12]. Table 5 shows the frequency convergence of a SSFF plate, which does not have any trivial frequency. The first frequency is due to a combination of the rotational rigid-body SF beam modes from either direction. The second and the third frequencies are also nominal in magnitude, since there is a rotational-rigid-body SF beam mode contribution from one side. From the fourth frequency onwards, there are flexural contributions from either side dominating, causing the plate frequency to increase. They compare well with Leissa [12], and Dickinson, Blasio [7].

Table 6 shows the frequency convergence of the other boundary conditions possible through the elastically supported edges, i.e. SFSF, SSSF, and SSSS. For the SFSF plate, the first frequency has the product of the first SS beam flexural mode and the FF beam translational rigid-body mode dominating. The second frequency has the first SS beam flexural mode combined with the FF beam rotational rigid-body mode dominating. Thus, these two frequencies are again nominal in magnitude. Then onwards, the flexural modes from either direction start gaining prominence, and hence, the plate frequency increases. For the SSSF plate, the first frequency has the product of the first SS beam flexural mode and the SF beam rotational rigid-body mode dominating. From then onwards, there is flexure dominating from either side, leading to higher frequencies. They compare well with Leissa [12] and Mizusawa [16].

Table 3. Convergence studies of square FFFF Plate.

FFFF	ω_1	ω_2	ω_3	ω_4	ω_5	ω_6	ω_7	ω_8	ω_9	ω_{10}	ω_{11}	ω_{12}	ω_{13}
Mode	(1, 1)	(1, 2)	(2, 1)	(2, 2)	(1, 3)	(3, 1)	(2, 3)	(3, 2)	(1, 4)	(4, 1)	(3, 3)	(2, 4)	(4, 2)
R (2×2)	0.0006	0.00089	0.00089	14.1985	–	–	–	–	–	–	–	–	–
R (3×3)	0.0006	0.00089	0.00089	14.1985	19.922	24.532	36.494	36.494	–	–	67.246	–	–
R (4×4)	0.0006	0.00089	0.00089	13.535	19.922	24.532	35.3305	35.331	61.808	61.808	67.246	69.788	78.500
R (5×5)	0.0006	0.00089	0.00089	13.535	19.789	24.432	35.1231	35.123	61.534	61.534	64.272	69.788	78.500
R (6×6)	0.0006	0.00089	0.00089	13.488	19.789	24.432	35.0234	35.023	61.526	61.526	64.272	69.762	77.825
Theory	0.0002	0.0003	0.0003	13.488	19.789	24.432	35.023	35.023	61.526	61.526	64.272	69.762	77.825
LEISSA [12]	–	–	–	13.489	19.789	24.432	35.024	35.024	61.526	–	–	–	–
DICKINSON, BLASIO [7]	–	–	–	13.468	19.596	24.270	–	–	–	–	–	–	–
MONTERRUBIO, IIANKO [17]	–	–	–	13.468	19.596	24.270	34.801	34.801	61.093	–	–	–	–

'R' refers to plate with translational edge restraints.

Table 4. Convergence studies of square SFFF Plate.

SFFF	ω_1	ω_2	ω_3	ω_4	ω_5	ω_6	ω_7	ω_8	ω_9	ω_{10}	ω_{11}	ω_{12}	ω_{13}
Mode	(1, 1)	(1, 2)	(2, 1)	(2, 2)	(1, 3)	(3, 1)	(2, 3)	(3, 2)	(4, 1)	(1, 4)	(3, 3)	(2, 4)	(4, 2)
R (2×2)	0.0006	6.7222	15.418	26.465	–	–	–	–	–	–	–	–	–
R (3×3)	0.0006	6.695	15.089	26.082	26.249	49.007	51.623	60.930	–	–	91.719	–	–
R (4×4)	0.0006	6.653	15.088	25.559	26.199	48.931	51.415	59.233	65.708	89.937	90.374	104.222	114.274
R (5×5)	0.0006	6.651	15.023	25.539	26.145	48.723	50.868	59.220	65.620	88.535	89.799	103.784	114.219
R (6×6)	0.0006	6.648	15.023	25.492	26.125	48.711	50.849	59.150	65.526	88.442	89.411	103.782	114.016
Theory	0.0006	6.648	15.023	25.491	26.126	48.711	50.849	59.150	65.5269	88.442	89.4118	103.7826	114.017
LEISSA [12]	–	6.648	15.023	25.492	26.126	48.711	50.849	–	–	–	–	–	–

'R' refers to plate with translational edge restraints.

Table 5. Convergence studies of square SSFF Plate.

SSFF	ω_1	ω_2	ω_3	ω_4	ω_5	ω_6	ω_7	ω_8	ω_9	ω_{10}	ω_{11}	ω_{12}	ω_{13}
Mode	(1, 1)	(1, 2)	(2, 1)	(2, 2)	(1, 3)	(3, 1)	(3, 2)	(2, 3)	(4, 1)	(1, 4)	(3, 3)	(2, 4)	(4, 2)
R (2×2)	3.384	17.446	19.624	40.111	–	–	–	–	–	–	–	–	–
R (3×3)	3.372	17.440	19.456	38.590	51.429	53.954	73.460	76.294	–	–	116.702	–	–
R (4×4)	3.370	17.428	19.406	38.373	51.389	53.835	73.172	75.246	105.407	107.8275	113.724	127.212	129.989
R (5×5)	3.369	17.417	19.382	38.313	51.355	53.777	73.112	74.980	105.345	107.7538	113.081	127.104	129.429
R (6×6)	3.369	17.407	19.367	38.291	51.324	53.738	73.097	74.873	105.293	107.705	112.853	127.076	129.246
Theory	3.369	17.406	19.367	38.291	51.324	53.738	73.097	74.874	105.293	107.706	112.854	127.077	129.247
Leissa [12]	3.369	17.407	19.367	38.291	51.324	53.738	–	–	–	–	–	–	–
Dickinson, Blasio [7]	3.367	17.316	19.293	–	–	–	–	–	–	–	–	–	–

'R' refers to plate with translational edge restraints.

Table 6. Convergence studies of square plates with other boundary conditions.

		ω_1	ω_2	ω_3	ω_4	ω_5	ω_6	ω_7	ω_8	ω_9	ω_{10}
SFSF	Mode	(1,1)	(1,2)	(1,3)	(2,1)	(2,2)	(2,3)	(1,4)	(3,1)	(3,2)	(4,1)
R		9.7080	16.19204	36.7452	39.2126	47.0347	70.877	75.2994	88.5081	96.71145	111.1647
Theory		9.688	16.192	36.7398	39.1570	47.0347	70.8501	75.2994	88.4185	96.7114	111.1647
	Leissa [12]	9.7600	16.1348	36.7256	38.9450	46.7381	70.7401	75.2834	87.9867	96.0405	–
SSSF	Mode	(1,1)	(1,2)	(2,1)	(2,2)	(1,3)	(3,1)	(2,3)	(3,2)	(1,4)	(4,1)
R		11.7373	27.7682	41.4120	59.150	61.8667	90.7404	94.5378	109.1333	115.6933	145.7803
Theory		11.7373	27.7682	41.4120	59.150	61.8667	90.7404	94.5378	109.1333	115.6933	145.7803
	Mizusawa [16]	11.68	27.76	41.20	59.07	61.86	–	–	–	–	–
	Leissa [12]	11.6845	27.7563	41.1967	59.0655	61.8606	90.2941	94.4837	108.9185	115.6857	–
SSSS	Mode	(1,1)	(1,2)	(2,1)	(2,2)	(1,3)	(3,1)	(2,3)	(3,2)	(1,4)	(4,1)
R		19.7391	49.34724	49.3472	78.9551	98.6925	98.6925	128.30	128.30	167.772	167.7728
	Leissa [12]	19.7392	49.3480	49.3480	78.9568	98.6960	98.6960	128.3049	128.3049	167.7833	–

'R' refers to plate with translational edge restraints.

Table 7. FFFF plate modeshapes with rigid-body beam-wise participation.

Mode	Ma, Huang [15]	Present method	Frequency parmeters	Mode	Ma, Huang [15]	Present method	Frequency parmeters
		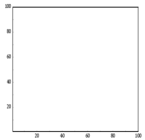	0.000	Mode 13	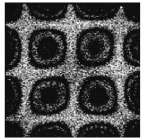	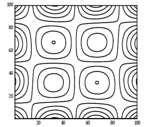	154.361
		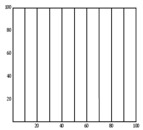	0.000	Mode 14	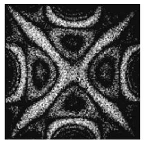	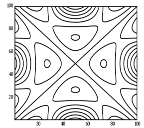	161.993
		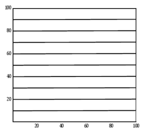	0.000	Mode 15	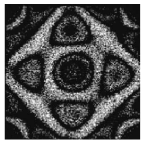	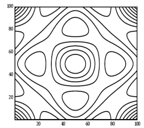	169.852
Mode 1	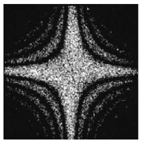	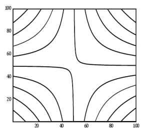	13.488	Mode 16	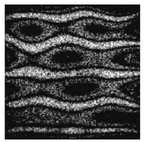		
Mode 2	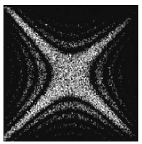	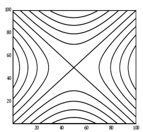	19.736	Mode 17	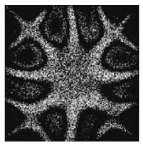	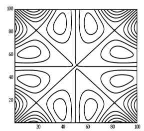	205.717

Table 7. [Cont.].

Mode	Ma, Huang [15]	Present method	Frequency parmeters	Mode	Ma, Huang [15]	Present method	Frequency parmeters
Mode 3	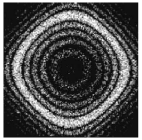	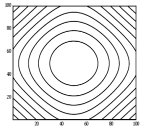	24.390	Mode 18	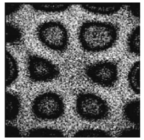	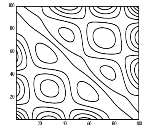	217.330
Mode 4	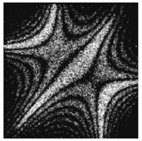	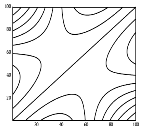	34.995	Mode 19	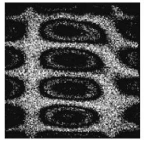		
Mode 5	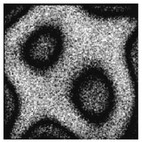	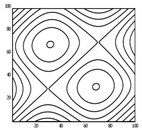	61.420	Mode 20	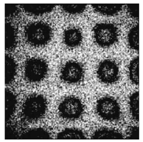	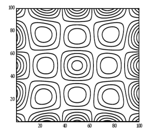	283.797
Mode 6	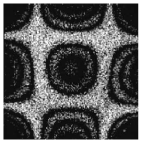	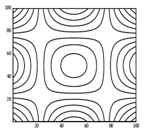	63.938	Mode 21	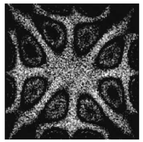	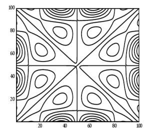	293.842
Mode 7	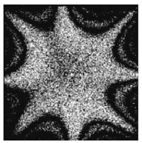	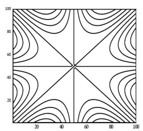	69.762	Mode 22	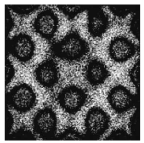	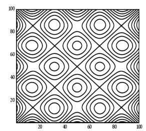	295.436

Table 7. [Cont.].

Mode	MA, HUANG [15]	Present method	Frequency parmeters	Mode	MA, HUANG [15]	Present method	Frequency parmeters
Mode 8	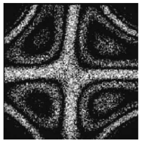	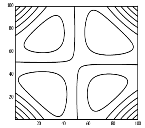	77.825	Mode 23	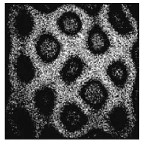	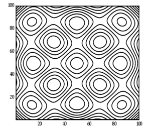	301.299
Mode 9	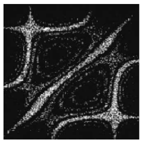	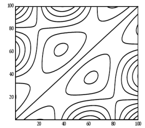	106.064	Mode 24	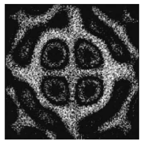	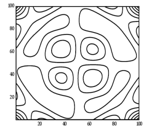	305.178
Mode 10	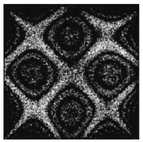	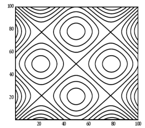	117.789	Mode 25	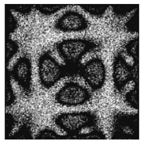	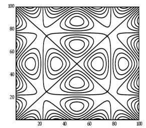	337.799
Mode 11	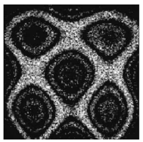	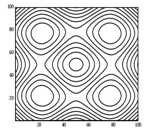	122.947	Mode 26	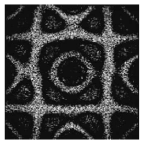	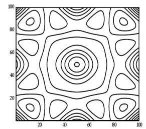	348.058
Mode 12	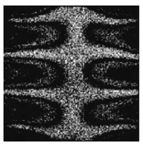			Mode 27	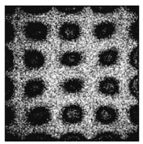	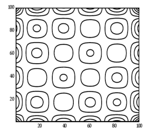	466.810

Table 7 shows the contours of the modeshapes of a square FFFF plate, generated from the eigen vector. The first three modeshapes show no flexure in their contours, suggesting zero natural frequencies. The mode 1 shows the strong participation of rotational rigid-body modes from either direction. The mode 2, mode 3, mode 4, mode 5, mode 7, mode 8, mode 9, mode 10, mode 11, mode 13, mode 17, mode 22, mode 23 and mode 24 show the participation of rigid-body mode from one direction. The mode 6, mode 14, mode 15, mode 20, mode 21, mode 25, mode 26 and mode 27 show the flexural modes from either direction. The modeshapes obtained from present rigid-body modes and coupled with beam functions in the Rayleigh-Ritz method. The results obtained are well matched with experimental work by Ma and Huang [15] and Chen *et al.* [5]. These modeshapes need the rigid-body beam-wise modal participation in order to manifest. Physically mode 12, mode 16 and mode 19 appear on the plate experimentally. However, mathematically eigenvector is insufficient to replicate

Table 8. Study of FFFF plate modeshapes through eigen vector.

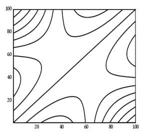

34.995

Eigen vector

0	0	0	0.01	0	0
0	0	−0.80	0	0.02	0
0	1	0	0.001	0	0
0	0	−0.01	0	0	0
0	−0.025	0	0	0	0
0	0	0	0	0	0

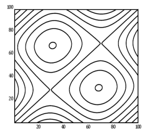

61.420

Eigen vector

0	0	0	0.08	0	0
0	0	1	0	−0.5	0
0	−0.70	0	0	0	0
−0.125	0	0	0	0	0
0	0.357	0	0.002	0	0
0	0	0	0	0	0

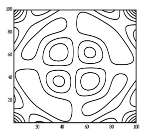

305.178

Eigen vector

0	0	0	0	0	0
0	−1	0	0.098	0	−0.47
0	0	0	0	0	0
0	0.098	0	−0.018	0	0.08
0	0	0	0	0	0
0	−0.47	0	0.083	0	0.029

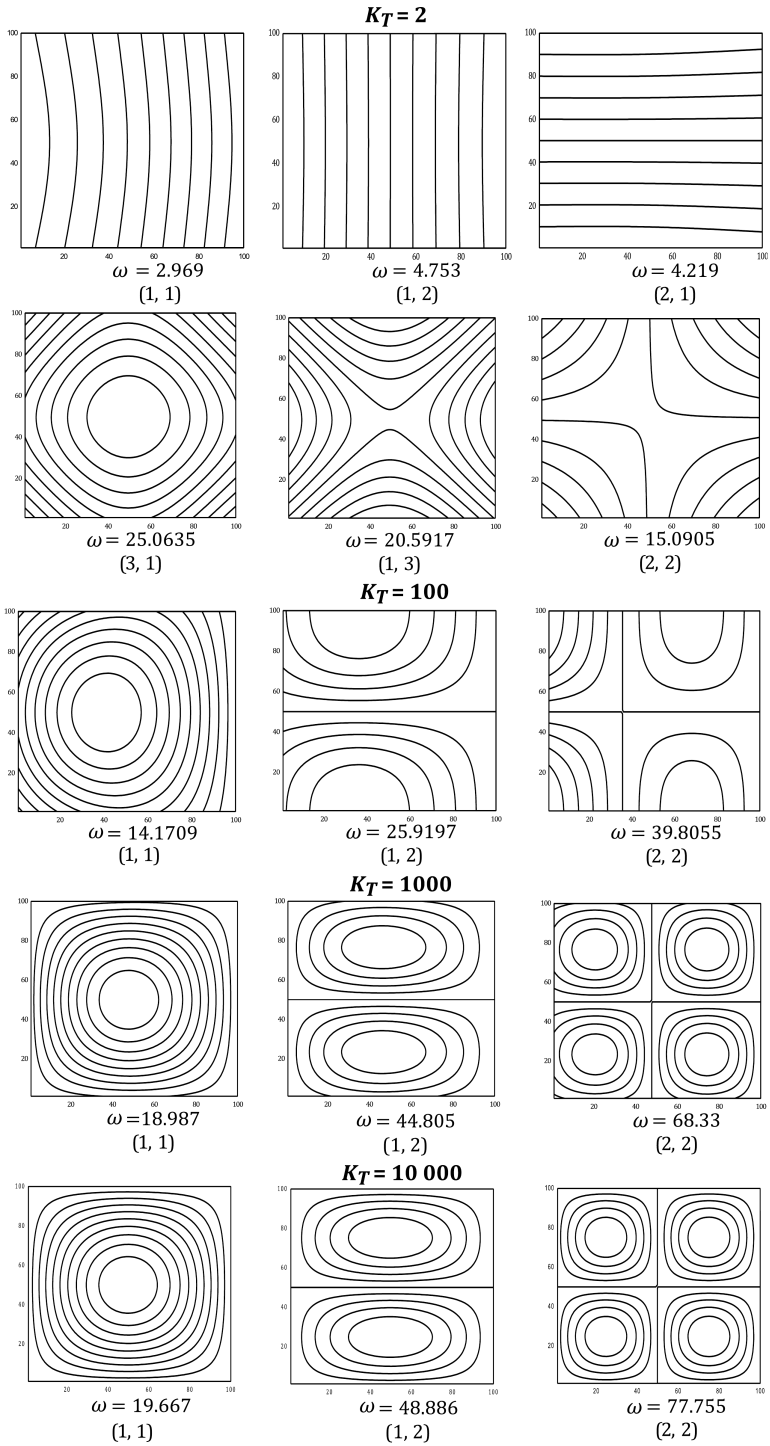

FIG. 10. TTTT square plate modeshapes for different values of K_T.

these modeshapes. The participation of these rigid-body modes in FFFF plate is crucial in determining the plate modeshapes and the plate natural frequency correctly.

Table 8 demonstrates the important of rigid-body modes in FFFF plate. The study is done through eigen vector analysis, the frequency parameters of mode 4, mode 9 and mode 24 are found to be 34.995, 61.420 and 305.178. However, there eigen vector is tabulated in Table 8. in all three modeshapes there is a strong participation of rotational rigid-body mode from one side which is clearly seen in eigen vector table. In FFFF plate the rigid-body modes play an important role in determining the exact shape of the plate at particular frequency.

Figure 10 shows the modeshapes for different value of K_T by simultaneously varying all the four edges of TTTT square plate. For a lower value of K_T (e.g., $K_T = 2$). The results obtained is verified with Saha *et al.* [21] for lower value of K_T (e.g., $K_T = 2$). The first six modes show the participation of rigid- body modes. However, the first row shows the participation of rigid body modes from both the directions (e.g., (1, 1), (1, 2), (2, 1)). The second row shows the participation of rigid mode from one direction and flexural mode from other direction (e.g., (3, 1), (1, 3)). The second row also shows the strong participation of rotational mode from both directions (e.g., (2, 2)). Moreover, some of the transition modes are also shown in row three and row four for higher translational spring constants ($K_T = 1e2, 1e3$). For a relatively higher value of ($K_T = 1e4$), the plate behaves like simply supported which is clearly seen in row five.

3.4. Comparison of present rigid body modes with Monterrubio, Ilanko [17] *and* Li [13, 14]*: in the Rayleigh-Ritz method*

3.4.1. Set of a complete admissible functions. The following sets of complete admissible functions are used in present paper:

- translational mode:

$$\phi_1(x) = 0.5\cos\beta_T x + 0.5\cosh\beta_T x, \tag{3.1$_1$}$$

- rotational mode

$$\phi_2(x) = 0.5\cos\beta_R x - \frac{1}{\beta_R L}\sin\beta_R x + 0.5\cosh\beta_R x - \frac{1}{\beta_R L}\sinh\beta_R x. \tag{3.1$_2$}$$

The value for $\beta_T = 0$, $\beta_R = 0.01$ (any value less than or equal to $\beta_R \le 10^{-2}$).

- lowest order polynomial:

$$\phi_3(x) = \left(\frac{x}{L}\right)^2, \tag{3.1$_3$}$$

- same cosine function used by Monterrubio, Ilanko [17] and Li [13, 14]:

$$\phi_i = \cos\left(\frac{i-3}{L}\right)\pi x, \qquad (i = 4, 5, 6, 7, \dots, n)\,. \tag{3.1$_4$}$$

Figure 11 shows the first five mode shapes of present set. The first and second functions are exact modes of the free-free beam. However, these functions satisfy the natural boundary condition of the zero bending moment and shear force. Moreover, these mode shapes have zero curvature which is illustrated above clearly. The third function is a simple polynomial $\left(\frac{x}{L}\right)^2$ of degree 2 which represent the constant curvature. From, the fourth function onwards, it is a cosine series, which is an exact mode of a GG (sliding-sliding/guided-guided) beam. The proof of convergence of this cosine function is demonstrated by Monterrubio and Ilanko [17]. Furthermore, the effects of these trial functions on the geometric boundary conditions of the beam are as follows:

(i) $\phi_i(0) \neq 0$ This action is satisfied by Eqs. $(3.1)_1$, $(3.1)_2$ and $(3.1)_4$.

(ii) $\phi_i(L) \neq 0$ This action is satisfied by all the functions $(3.1)_1$–$(3.1)_4$.

(iii) $\left.\frac{\partial \phi_i}{\partial x}\right]_{x=0} \neq 0$ This action is satisfied by Eqs. $(3.1)_2$.

(iv) $\left.\frac{\partial \phi_i}{\partial x}\right]_{x=L} \neq 0$ This action is satisfied by Eqs. $(3.1)_2$ and $(3.1)_3$.

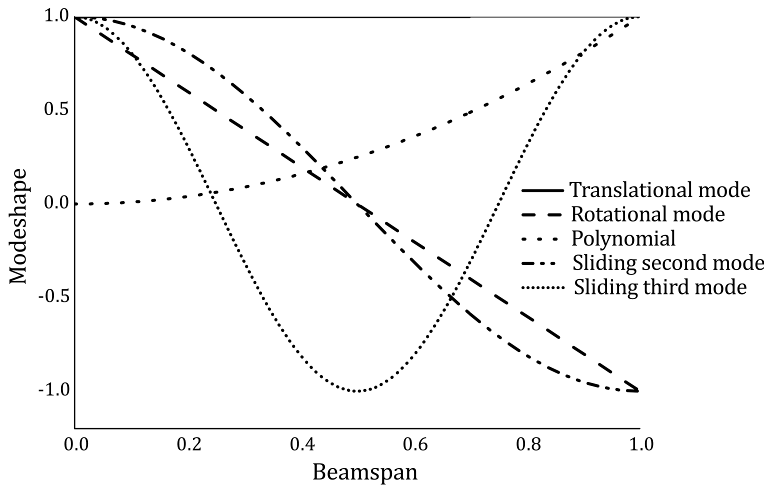

Fig. 11. First five modeshapes of present admissible functions.

The above action shows that a suggested trial function is a complete set, with non-zero slope and displacement. Therefore, these sets are able to form the deflection of the FF beam. The combination of these functions models the complete set of admissible functions for unconstrained structure (free-free beam).

BUDIANSKY and HU [4] stated that, it is sufficient to satisfy the geometric boundary conditions as a whole set of admissible functions rather than to satisfy geometric boundary conditions individually for each function. Moreover, for other constrained structure geometric boundary conditions are imposed by rotational and translational restrained at both ends of the beam.

3.4.2. Difference between MONTERRUBIO, ILANKO [17] *and this paper.* The main difference between approach of MONTERRUBIO and ILANKO [17] and this paper are as follows:

a) The present approach has been used the exact translational and rotational modeshapes derived mathematically from the Taylors series expansion. Additionally, these modeshapes are orthogonal with respect to other functions. By the relationship mentioned by SZILARD [18].

$$\int_0^{\text{beam span}} \cos\frac{i\pi x}{L}\cos\frac{j\pi x}{L}\,\mathrm{d}x = \left\{\begin{array}{cc} 0 & \text{for } \ i \neq j \\ \dfrac{\text{beam span}}{2} & \text{for } \ i = j \end{array}\right\}.$$

b) MUKHOPADHYAY [18] stated that the importance of orthogonality in choosing the admissible functions is that the magnitude of non-diagonal terms in the stiffness and mass matrices should be small.

c) Tables 9 and 10 present the comparison of mass and stiffness matrices for unconstrained structure. Therefore, the first three set of admissible functions are considered in the RRM and compared with MONTERRUBIO, ILANKO [17]. However, the matrices from present set of admissible functions are more sparse than presented by MONTERRUBIO and ILANKO [17], this is highlighted in Tables 9 and 10. This is because; the first two admissible functions of present set are exact translational and rotational beam modeshapes which is derived from the Taylors series expansion. Furthermore, some of the functions are orthogonal with respect to other function (i.e. cosine function), which leads to the more zeros in the off-diagonal positions and strong diagonally dominant matrices.

d) The main advantage of the orthogonal functions is that the fewer number of functions is sufficient for fast convergence in the RRM, without producing any round-off error in the solution.

e) The third admissible function onwards, the simple polynomial and cosine function are considered in order to complete the set of admissible functions; as considered by MONTERRUBIO and ILANKO [17]. The cosine function is also orthogonal by the relationship mentioned by SZILARD [23].

Table 11 shows the first six frequency parameters for FFFF plate. However, the RRM is utilised to calculate the frequency parameters with present set of admissible functions. The results obtained are well matched with Monterrubio, Illanko [17]. Only 25 functions in both directions are sufficient for the convergence. The results are accurate up to four places of decimal without producing any numerical instability.

Table 9. Comparison of mass matrix for unconstrained structure.

Monterrubio and Ilanko [17]								
0	0	0	0	0	0	0	0	0
0	0	0	0	0	0	0	0	0
0	0	4	0	0	2	1.2	0.6	1.7
0	0	0	0	0	0	0	0	0
0	0	0	0	1.4	1.4	0	1.4	1.4
0	0	2	0	1.4	3.2	0.6	1.7	3.0
0	0	1.2	0	0	0.6	4	2	1.7
0	0	0.6	0	1.4	1.7	2	3.2	3.0
0	0	1.7	0	1.4	3.0	1.7	3.0	4.3
Present method								
0	0	0	0	0	0	0	0	0
0	0	0	0	0	0	0	0	0
0	0	4	0	0	**0**	1.2	**0**	1.7
0	0	0	0	0	0	0	0	0
0	0	0	0	22.4	−11.2	0	−11.2	5.6
0	0	**0**	0	−11.2	8.8	**0**	5.6	−4.4
0	0	1.2	0	0	**0**	4	**0**	1.7
0	0	**0**	0	−11.2	5.6	0	8.8	−4.4
0	0	1.7	0	5.6	−4.4	1.7	−4.4	4.3

Table 10. Comparison of stiffness matrix for unconstrained structure.

Monterrubio and Ilanko [17]								
1	0.5	0.33	0.5	0.25	0.166	0.33	0.166	0.11
0.5	0.33	0.25	0.25	0.166	0.125	0.166	0.11	0.083
0.33	0.25	0.2	0.166	0.125	0.1	0.11	0.083	0.066
0.5	0.25	0.16	0.33	0.166	0.11	0.25	0.125	0.083
0.25	0.166	0.12	0.166	0.11	0.083	0.12	0.083	0.062
0.16	0.125	0.1	0.11	0.083	0.066	0.083	0.062	0.05
0.33	0.166	0.11	0.25	0.125	0.083	0.2	0.1	0.066
0.16	0.11	0.083	0.125	0.083	0.0625	0.1	0.066	0.05
0.11	0.083	0.066	0.083	0.062	0.05	0.066	0.05	0.04

Table 10. [Cont.].

Present method								
1	**0**	0.33	**0**	**0**	**0**	0.33	**0**	0.11
0	0.33	−0.166	**0**	**0**	**0**	**0**	0.11	−0.055
0.33	−0.166	0.2	**0**	**0**	**0**	0.11	−0.055	0.066
0	**0**	**0**	0.33	**0**	0.11	−0.166	**0**	−0.055
0	**0**	**0**	**0**	0.11	−0.055	**0**	−0.055	0.027
0	**0**	**0**	0.11	−0.055	0.066	−0.055	0.027	−0.033
0.33	**0**	0.11	−0.166	0	−0.055	0.2	**0**	0.066
0	0.11	−0.055	**0**	−0.055	0.0277	**0**	0.066	−0.033
0.11	0.055	0.066	−0.055	0.027	−0.033	0.066	−0.033	0.04

Table 11. Convergence studies of $\left(\Omega^2 = \frac{\rho h \omega^2 a^4}{D}\right)$, for completely unconstrained (FFFF) plate.

# of terms	1	2	3	4	5	6
15 × 15	**13.469**	**19.596**	**24.2705**	**34.805**	**34.805**	**61.095**
20 × 20	**13.468**	**19.596**	**34.270**	**34.802**	**34.802**	**61.094**
25 × 25	**13.468**	**19.596**	**24.270**	**34.801**	**34.801**	**61.093**
$(40 \times 40)^c$	$(13.468)^b$	$(19.596)^b$	$(24.270)^b$	$(34.801)^b$	$(34.801)^b$	$(61.093)^b$

[c] Refers to the results taken from Monterrubio and Ilanko [17].

4. Conclusions

The study of free vibration of plates with free edges has been presented, using closed-form expression of the beam-wise orthogonal rigid-body modeshapes, which participate in the plate vibration. The presence and prominence of the rigid-body modes, over a wide range of translational edge spring stiffness, is difficult to comprehend. This has indirectly been done in this work by modeling the beam with translational edge restraints, and establishing the corresponding frequency parameters, wave numbers, and waveform coefficients. Extreme values of the spring constant lead to the classical edges.

Mathematically generated closed-form modeshapes for translational and rotational rigid body modes of the corresponding classical beams, i.e. FF and SF beams, are presented and compared with translationally restrained beam modeshapes. The rigid-body beam modes have a non-negligible contribution into the plate frequency, though they themselves have zero frequency. The presence of rigid-body beam modeshapes causes a few trivial plate natural frequencies to exist, and along with a few of nominal magnitudes. Their accuracy in terms of zero curvature, orthogonality and boundary conditions cannot be compromised on. This necessitates a mathematical attempt to establish the classical free-free and hinged-free rigid-body modeshapes. The frequency equation of the beam precipitates the trivial and non-trivial frequency parameters, leading to the corresponding waveform coefficients and thus, modeshapes. For the beam with both ends translationally supported (TT beam), the rotational rigid-body mode jumps to the flexural mode with increasing spring constant. This tells the unpredictable nature of FF beam/FFFF plate frequencies, especially in the range of non-D edge spring constant $10^1 < K_T < 10^2$. However, a smooth transition is noticed for the ST beam.

Closed-form modes are seen to give accurate results of the plate natural frequencies when used in the Rayleigh-Ritz method. The accuracy is consistently maintained for plates with all possible combinations/permutations of free and simply-supported edges. The mathematical modeshapes of the classical FF and SF beams participate in the Rayleigh-Ritz method to generate the same plate natural frequency when we use the rigid-body modeshapes generated through the non-classical edges and then the spring constant is assumed to be very small $K_T < 10^{-7}$. This self-verification proves the efficacy of the closed-form classical rigid-body beam modeshapes suggested uniquely in this work. The methodology of generating closed-form classical rigid-body modes can be made applicable in more complex structures with one or more free edges, e.g. structures with taper, intermediate supports, axial loads, etc. The frequencies of non-classically supported plates can be known directly from these results.

We have proposed to use the closed-form expression of beam-wise orthogonal rigid-body mode shapes that can account for the translational vibration characteristics of the plate with free edges. Comprehensive numerical examples have been given to demonstrate the effectiveness of the proposed method by comparing numerical results to those in literature. The current method may provide a new alternative to treat Kirchhoff plates with free edges, which are known for their notoriety in vibration analysis, both numerically and experimentally.

References

1. Bardell N.S., *Free vibration analysis of a flat plate using the hierarchical finite element method*, Journal of Sound and Vibration, **51**(2): 263–289, 1991.

2. Bassily S.F., Dickinson S.M., *On the use of beam functions for problems of plates involving free edges*, Journal of Applied Mechanics, **42**(4): 858–864, 1975.

3. Bhat R.B., *Natural frequencies of rectangular plates using characteristic orthogonal polynomials in Rayleigh-Ritz method*, Journal of Sound and Vibration, **102**(4): 493–499, 1985.

4. Budiansky B., Hu P.C., *The Lagrangian multiplier method of finding upper and lower limits to critical stresses of clamped plates*, NASA Technical Report, NTIS Issue Number 199609, 1946.

5. Chen C.P., Huang C.H., Chen Y.Y., *Vibration analysis and measurement for piezoceramic rectangular plates in resonance*, Journal of Sound and Vibration, **326**(1–2): 251–262, 2009.

6. De Rosa M.A., Lippiello M., *Natural vibration frequencies of tapered beams engineering*, Engineering Transactions, **57**(1):45–66, 2009.

7. Dickinson S.M., Blasio A.D., *On the use of orthogonal polynomials in the Rayleigh-Ritz method for the study of the flexural vibration and buckling of isotropic and orthotropic rectangular plates*, Journal of Sound and Vibration, **108**(1): 51–62, 1986.

8. Dozio L., *On the use of the Trigonometric Ritz method for general vibration analysis of rectangular Kirchhoff plates*, Thin-Walled Structures, **49**: 129–144, 2011.

9. Eatock Taylor R., Ohkusu M., *Green functions for hydroelastic analysis of vibrating free–free beams and plates*, Applied Ocean Research, **22**(5): 295–314, 2000.

10. Hurlebaus S., Gaul L., *An exact series solution for calculating the eigenfrequencies of orthotropic plates with completely free boundary*, Journal of Sound and Vibration, **244**(5): 747–759, 2001.

11. Katsikadelis J.T., Armenakas A.E., *A new boundary equation solution to the plate problem*, ASME Journal of Applied Mechanics, **56**(2): 364–374, 1989.

12. Leissa A.W., *The free vibration of rectangular plates*, Journal of Sound and Vibration, **31**(3): 257–293, 1973.

13. Li W.L., *Comparison of Fourier sine and cosine series expansions for beams with arbitrary boundary conditions*, Journal of Sound and Vibration, **255**(1), 185–194, 2002.

14. Li W.L., *Vibration analysis of rectangular plates with general elastic boundary supports*, Journal of Sound and Vibration, **273**(3): 619–635, 2004.

15. Ma C.C., Huang C.H., *Experimental whole-field interferometry for transverse vibration of plates*, Journal of Sound and Vibration, **271**(3–5): 493–506, 2004.

16. Mizusawa T., *Natural frequencies of rectangular plates with free edges*, Journal of Sound and Vibration, **105**(3): 451–459, 1986.

17. Monterrubio L.E., IIanko S., *Proof of convergence for a set of admissible functions for the Rayleigh-Ritz analysis of beams and plates and shells of rectangular planform*, Computers and Structures, **147**(C): 236–243, 2015.

18. Mukhopadhyay M., *Structural dynamics: vibrations & systems*, Ane Books India, 2008.

19. Rao C.K., Mirza S., *A note on vibrations of generally restrained beams*, Journal of Sound and Vibration, **130**(3): 453-465, 1989.

20. Rao L.B., Rao C.K., *Vibrations of circular plate supported on a rigid concentric ring with transnational restraint boundary*, Engineering Transactions, **64**(3): 259–269, 2016.

21. Saha K.N., Kar R.C., Datta P.K., *Free vibration analysis of rectangular Mindlin plates with elastic restraints uniformly distributed along the edges*, Journal of Sound and Vibration, **192**(4): 885–904, 1996.

22. Saha K.N., Misra D., Pohit G., Ghosal S., *Large amplitude free vibration study of square plates under different boundary conditions through a static analysis*, Journal of Vibration and Control, **10**(7): 1009–1028, 2004.

23. Szilard R., *Theories and applications of plate analysis: classical numerical and engineering method*, John Wiley & Sons, 2004.

24. Tang Y., *Numerical evaluation of uniform beam modes*, Journal of Engineering Mechanics, **129**(12): 1475–1477, 2003.

25. Warburton G.B., Edney S.L., *Vibrations of rectangular plates with elastically restrained edges*, Journal of Sound and Vibration, **95**(4): 537–552, 1984.

26. Xiang Y., Liew K.M., Kitipornchai S., *Vibration analysis of rectangular Mindlin plates resting on elastic edge supports*, Journal of Sound and Vibration, **204**(1): 1–16, 1997.

27. Zhou D., *Natural frequencies of elastically restrained rectangular plates using a set of static beam functions in the Rayleigh-Ritz method*, Computers and Structures, **57**(4): 731–735, 1995.

Received November 5, 2017; accepted version January 3, 2018.